We are IntechOpen, the world's leading publisher of Open Access books Built by scientists, for scientists

6,000
Open access books available

148,000
International authors and editors

185M
Downloads

Our authors are among the

154
Countries delivered to

TOP 1%
most cited scientists

12.2%
Contributors from top 500 universities

CLARIVATE ANALYTICS
BOOK CITATION INDEX
INDEXED

WEB OF SCIENCE™

Selection of our books indexed in the Book Citation Index in Web of Science™ Core Collection (BKCI)

Interested in publishing with us?
Contact book.department@intechopen.com

Numbers displayed above are based on latest data collected.
For more information visit www.intechopen.com

Chapter

Perspective Chapter: Design and Characterization of Natural and Synthetic Soft Polymeric Materials with Biomimetic 3D Microarchitecture for Tissue Engineering and Medical Applications

Ching-Cheng Huang and Masashi Shiotsuki

Abstract

Continuous work and developments in biomedical materials used in three-dimensional (3D) bioprinting have contributed to significant growth of 3D bioprinting applications in the production of personalized tissue-repairing membrane, skin graft, prostheses, medication delivery system, and 3D tissue engineering and regenerative medicine scaffolds. The design of clinic products and devices focus on new natural and synthetic biomedical materials employed for therapeutic applications in different 3D bioprinting technologies. Design and characterization of natural and synthetic soft polymeric materials with biomimetic 3D microarchitecture were considered. The natural soft polymeric materials would focus on new design bioinspired membranes containing supercritical fluids-decellularized dermal scaffolds for 3D bioprinting potential applications. Synthetic soft polymeric materials would focus on bioinspired polyvinyl alcohol (b-PVA) matrix with structural foam-wall microarchitectures. Characterization, thermal stability, and cell morphology of the b-PVA and the corresponding collagen-modified b-PVA were employed to evaluate their potential tissue engineering applications. Also, the b-PVA materials were conductive to HepG2 cells proliferation, migration, and expression, which might serve as a promising liver cell culture carrier to be used in the biological artificial liver reactor. TGA, DTG, DSC, SEM, and FTIR were employed to build up the effective system identification approach for biomimetic structure, stability, purity, and safety of target soft matrix.

Keywords: biomimetic, three-dimensional, microarchitecture, design-thinking, supercritical fluids

1. Introduction

Bioprinting, a type of three-dimensional (3D) bioprinting, uses cells and other biological materials as "inks" to fabricate 3D biological structures. Bioprinted materials have the potential to repair damaged organs, cells, and tissues in the human body. Skin, bone, and blood vessels may be bioprinted. Although a variety of tissue engineering strategies combining cells and biomaterial scaffolds have been investigated for human tissues regeneration (e.g., using natural biomaterials and/or synthetic polymers [1]), the success of this approach still strongly depends on the development of more suitable scaffolds. In this sense, one of the main challenges is to accurately reproduce the complex 3D anatomy with personalized shape and size [2–4]. Efforts to address these issues have led to an increased interest in the application of three-dimensional (3D) bioprinting in the tissue engineering field. 3D bioprinting is a biofabrication method that uses computer-aided design (CAD) and additive layer manufacturing technique to precisely deposit bioinks (basically comprising a mixture of biomaterials with cells, with or without bioactive molecules) in a predesigned manner to create 3D bioengineered living structures and to generate artificial tissue and organs [5, 6]. Using this novel printing technology, biomaterials were possible to fabricate a patient-specific scaffold reproducing individual shape, size, and macrostructure of the native tissue [7, 8]. An implant's effectiveness depends upon the form of biomaterial used in its manufacture. A suitable material for implants should be biocompatible, sterile, mechanically stable, and simple to shape [9]. 3D printing technologies have been breaking new ground in the medical industries in order to build patient-specific devices embedded in bioactive drugs, cells, and proteins. 3D printing was a non-exclusive concept that defines various techniques for layer-by-layer construction. 3D bioprinting has progressed the method of printing standard biocompatible materials and even actual cells into difficult 3D dimensional tissue buildings [10], with the ability to create ideal tissues and organs appropriate for different biomedical uses, such as organ transplantation [11]. In recent years, many bioprinting techniques have been developed to store cells and hydrogels together, altered and used as cell printers to print polymers [12]. In such printers, cell suspensions or cell totals are mounted on printer extruder, and the printing mechanism is controlled. Continuous work and developments in biomaterials used in 3D printing have contributed to significant growth of 3D printing applications in the production of personalized tissue-repairing membrane, skin graft, prostheses, medication delivery system, and 3D tissue engineering and regenerative medicine scaffolds. The design of clinic products and devices focus on new natural and synthetic biomedical materials used for therapeutic applications in different 3D bioprinting technologies. Many specific forms of medical 3D bioprinting technology are explored in depth, including extrusion-based bioprinting and inkjet printing processes, the specific therapeutic uses, various types of biomaterial used today, and the major shortcomings are being studied in depth.

Bioinspired structure-guided tissue/cell in vivo growth or vitro culturing tissue/cell in vivo growth and in vitro culturing are remarkably important for implantable medical devices and drug evaluation [13]. To achieve desired growth and reproduction, it is necessary to construct the culturing conditions and the growing structure as close to living being as possible. Bioinspired surface was applied to the implants to improve the implanting quality. Bioinspired porous structure was built on the scaffolds to guide and improve the tissue growth.

2. Design and preparation of natural soft polymeric materials with biomimetic 3D microarchitecture containing decellularized extracellular matrix

Tree-dimensional (3D) bioprinting showed potential in tissue engineering and regenerative applications due to its overwhelming advantages over other approaches. In order to promote the functions of bioprinted tissues, the development of novel and versatile bioinks will have crucial implications [14]. Natural materials were famous for the excellent biocompatibility and abundance, among which sodium alginate mixed with gelatin has been widely used as bioink for extrusion-based 3D bioprinting [15]. Despite advance in bioprinting and bio-fabrication during the past decade, fabricating complex and functional tissue constructs that mimic their natural counterparts still remains a challenge. Bioink optimization is considered as one of main challenges in cell-laden 3D bioprinting [16].

Numerous materials have been proposed, modified, and employed for medical bioprinting applications such as scaffolds for skin and bone tissue reconstruction such as synthetic materials and natural materials [17–29]. In bioprinting applications, biomedical materials could be extruded through a print head either by pneumatic pressure or mechanical force. Since the process did not involve any heating procedures, it was most commonly used for preparing tissue engineering constructs with cells and growth hormones laden. Bioinks were the biomedical materials laden with cells and other biological materials and used for 3D bioprinting. The 3D bioprinting process allowed for the deposition of small units of cells accurately, with minimal process-induced cell damage. Advantages such as precise deposition of cells control over the rate of cell distribution and process speed had greatly increased the applications of this technology in fabricating living scaffolds. A wide range of materials with varied viscosities and high cell density aggregates could be 3D printed using this technique. A large variety of polymers were under research for the use in bioprinting technology [18]. Natural polymers, including collagen [19], gelatin [20], decellularized extracellular matrix(dECM) [21], alginate [22], chitosan [23], cellulose [24], agarose [25], silk protein [26], and hyaluronic acid (HA) [27, 28], and photopolymerizable gelatin and hyaluronic acid [29] were commonly used in bioinks for 3D bioprinting (**Figure 1**). Often these bioinks are post-processed either by chemical or UV cross-linking to enhance the constructs' mechanical properties. Depending on the type of polymer used in the bioink, biological tissues and scaffolds of varied complexity can be fabricated.

Decellularized extracellular matrix (dECM) scaffolds had a lot of collagens, which constitute the main structural element of the dECM, provide tensile strength, regulate cell adhesion, support migration, and direct tissue development. Dense connective tissue is an abundant source of dECM scaffolds, which can be prepared and purified by a defatting and decellularizing procedure [21, 30]. The treatments combined with supercritical carbon dioxide and specific enzymes could be employed to prepare dECM scaffolds. Furthermore, a series of new biomedical composite materials containing dECM scaffolds and alginate could be designed and prepared for tissue engineering and bioprinting applications. The composite materials containing dECM scaffolds for biomimetic bioinks could be characterized by Fourier transform infrared spectroscopy (FTIR), thermo-gravimetric analysis (TGA), and scanning electron microscope (SEM) to get the results of identifications, thermal stabilities, and microstructures.

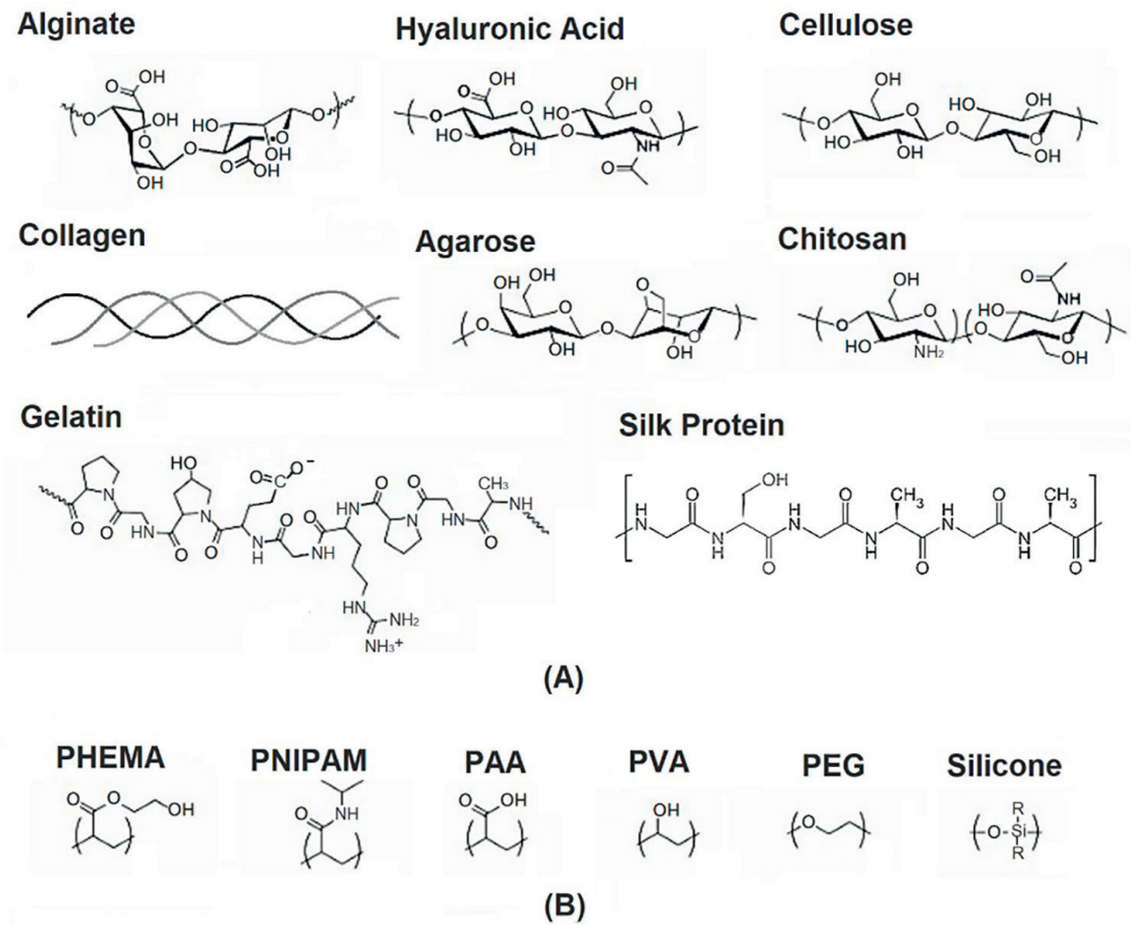

Figure 1.
Chemical structures of natural and synthetic soft polymeric materials with biomimetic 3D microarchitecture for tissue nanogineering, bioprinting, and medical applications. A) Natural soft polymeric material. B) Synthetic soft polymeric material.

2.1 Natural soft polymeric materials with biomimetic 3D microarchitecture containing decellularized extracellular matrix via supercritical fluid treatments

Decellularized extracellular matrix could be an important natural soft polymeric material with biomimetic 3D microarchitecture for bioprinting applications. In previous study, supercritical fluid of carbon dioxide ($ScCO_2$) was employed for preparation of designed decellularized extracellular matrix scaffolds for bioprinting applications. The $ScCO_2$ could be employed before or after decellularization treatments for effectively removing most fatty acids and tissues [21]. The $ScCO_2$ extraction could be performed for complete decellularization. Also, the steady thickness of about 0.5 mm of thinly sliced tissue sample, which could be obtained by using a designed tissue-cutting machine (Taiwan PARSD Pharm. Tech. Consulting Ltd Co.), was employed for complete decellularization.

Fourier transform infrared spectroscopy analysis was important for characterization of the natural soft polymeric material with biomimetic 3D microarchitecture containing decellularized extracellular matrix because of collagen segments, which could exhibit remarkable typical absorption bands of specific functional groups such as Amide I, Amide II, Amide III, Amide A, and Amide B could be an important for bioprinting applications. From the FTIR analysis of the original tissue such as porcine

skin, absorption bands at 1452, 1400, 1337, 1240, 1203, and 1080 cm^{-1} were attributed to the amides III containing $\delta(CH_2)$, $\delta(CH_3)$, ν(C–N), and δ(N–H) absorptions of collagens in the original porcine skin. Amides I and amides II absorptions were found at 1632 and 1551 cm^{-1}, respectively. The absorption band at 3301 cm^{-1} δ(C–H) was attributed to the fatty acid of the original porcine skin. The absorption band at 1744 cm^{-1} δ(C=O) was attributed to the fatty acid. After supercritical carbon dioxide treatment and decellularization, the decellularized extracellular matrix could be formed and the absorption bands of fatty acids could not be observed in FTIR spectrum, demonstrating the effectiveness of the supercritical carbon dioxide treatment and the formation of natural soft polymeric materials. The resulting natural soft polymeric materials could be considered as a nano-bioscaffold. The microstructures of resulting membranes with dNBS-S were characterized by scanning electron microscope (SEM). Scanning electron micrographs of the decellularized samples such as decellularized porcine skin (dNBS-S), decellularized porcine liver(dNBS-L), decellularized porcine costal cartilages (dNBS-CC), and decellularized porcine elastic cartilage (dNBS-EC) after treatment with supercritical carbon dioxide are shown in **Figure 2(A)–(D)**, respectively. The pore space of the resulting natural soft polymeric materials from different tissues such as the skin, liver, costal cartilage, and elastic cartilage with diameters in a range of 10–250 μm was observed, which could be good nano-bioscaffolds for cell migration [21].

Further, L929 cells were cultured on the resulting natural soft polymeric material for a potential evaluation of good nano-bioscaffolds for tissue engineering. The morphology of L929 cells cultured on the resulting natural soft polymeric materials was also investigated by SEM (**Figure 3**). Significantly, most area was covered by L929

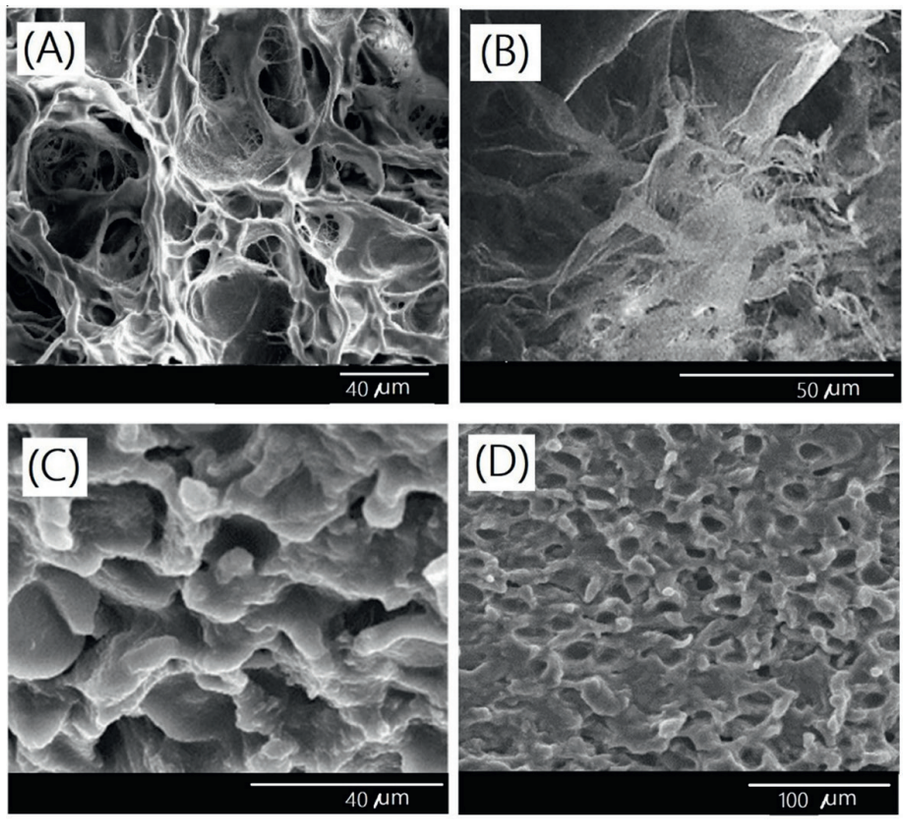

Figure 2.
Scanning electron micrographs of the samples: (A) decellularized porcine skin (dNBS-S), (B) decellularized porcine liver(dNBS-L), (C) decellularized porcine Costal cartilages(dNBS-CC), and (D) decellularized porcine elastic cartilage (dNBS-EC).

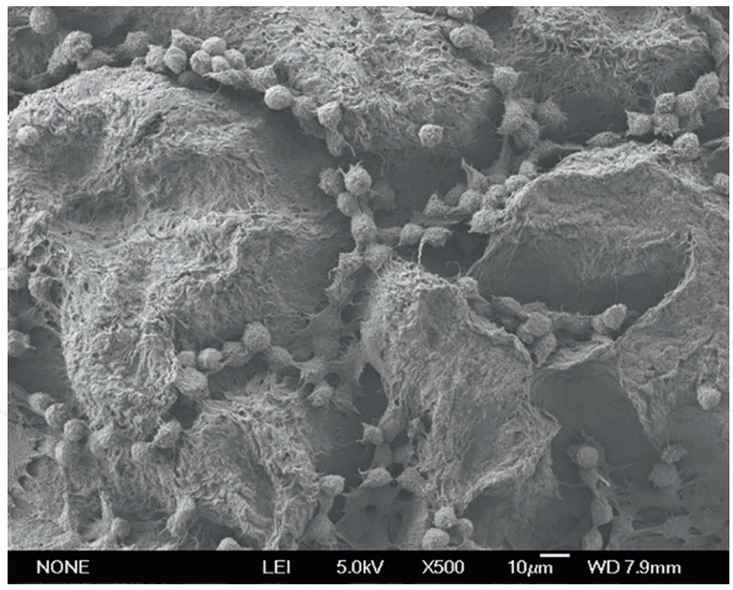

Figure 3.
SEM photograph of L929 cells grew on dNBS-S.

cells on the resulting natural soft polymeric materials such as dNBS-S after 3 days of culture was observed [21]. The cells that grew upon the dNBS-S were significantly observed. Perez-Puyana et al. also reported that the pore space of nano-bioscaffold was suggested to be small enough to establish a high specific surface area and large enough to allow cells to migrate into the microstructure (20–120 μm) [31].

2.2 Natural soft polymeric composite materials with biomimetic 3D microarchitecture containing alginate and decellularized extracellular matrix via supercritical fluid treatments

Decellularized extracellular matrix(dECM)/alginate composite materials with biomimetic 3D microarchitecture and cross-linked decellularized extracellular matrix/alginate composite materials with biomimetic 3D Microarchitecture could also be designed for tissue engineering and medical applications. Briefly, the desired amount of dECM powder was first dispersed completely in water. Then, alginate aqueous solution was homogenized thoroughly with the dispersed dECM solution. The alginate/dECM solutions were employed to form 3D printed membranes by using extrusion-based bioprinting, molding, and freeze-drying procedures for evaluation of new 3D bioprinting materials. Further, cross-linked decellularized extracellular matrix/alginate composite materials with biomimetic 3D Microarchitecture were designed and prepared by using ionic crosslinking procedure with $CaCl_2$ aqueous solution.

The incorporation of nano-bioscaffold(dNBS) in the alginate/decellularized extracellular matrix composite materials(AdNBS) with biomimetic 3D microarchitecture was done. The FTIR spectroscopy analysis was carried out to confirm the structures. In the spectrum of the AdNBS, the main absorption bands at around 1632 cm^{-1} (amide I, C-O, and C-N stretching), 1537 cm^{-1} (amide II) and 1242 cm^{-1} (amide III) were also observed. Because of the introduction of alginate segments, retaining the characteristic bands of pure sodium alginate was observed. The characteristic bands of AdNBS at around 1595 cm^{-1} (the carbonyl (C=O) bond) and 1408 cm^{-1} (asymmetric and symmetric stretching peaks of carboxylate salt groups) were visible [21].

It showed a stronger absorption band at 1595 cm^{-1} and two remarkably shoulders at 1632 and 1537 cm^{-1}, which were characteristic absorption of carbonyl groups of amide (amide I and amide II) of dNBS segments, which would confirm the formation of AdNBS composite materials remarkably. A higher absorption from 3600 to 3200 cm^{-1} would be observed in the spectrum, which suggested an increase of hydrogen bonds resulting from the interaction between dNBS molecule and alginate(ALG) molecule. The results of FTIR indicated the presence of dNBS in the composite materials as wells as the interaction between them. After cross-linking reaction, the cross-linked decellularized extracellular matrix/alginate composite materials with biomimetic 3D microarchitecture were obtained and the calcium alginate segments were formed. The -C-O-O-Ca-O-CO- structure made the C-O stretching vibration absorption increase and had an obvious absorption band at 1024 cm^{-1}, which indicated the formation of -CO-O-Ca-O-CO- structure in AdNBS materials [21].

The microstructure of resulting AdNBS composite materials was characterized by scanning electron microscopy (SEM). The micro-scaffold structure could be observed in the dNBS-S derived from porcine skin after treatment with supercritical carbon dioxide (**Figure 2(B)**) showed quite different morphology form ALG, which showed a micro-scaffold shape with narrow boundaries [21]. The averaged diameter of narrow boundaries was found in a range of 1–3 μm. The remarkable micro-scaffold structures were observed in AdNBS composite materials with various introduction ratios of dNBS-S and ALG. With the increasing introduction ratio of dNBS-S and ALG, the new combined micro-scaffold shapes of composite materials were observed with the spaces and smooth mixed boundaries. The averaged diameter of smooth mixed boundary was found in a range of 1–35 μm [21], which might provide relatively high structural and thermal stabilities.

Thermal stability of resulting natural soft polymeric materials with biomimetic 3D microarchitecture such as AdNBS-S could be evaluated by TGA (**Figure 4**). Thermogravimetric analysis of the ALG showed a maximum pyrolysis temperature (Tdmax) lower than 300 degrees. To enhance the thermal stability of ALG-based materials, the decellularized nano-bioscaffolds, dNBS-S, were introduced. The maximum pyrolysis temperature (Tdmax) of dNBS-S was higher than 300 degrees. The resulting AdNBS-S would be a new heat-resistant biomaterial for bioprinting applications. From TGA analysis of AdNBS-S, the main loss is presented in two different temperature ranges given by stage I(<150°C), stage II(150–250°C), and stage III (250–500°C). From TGA results of ALG, initial weight loss up to 150°C is found to be 15, 20, and 20 for non-cross-linked alginate(NCA), high cross-linked alginate(HCA) (5wt% $CaCl_{2(aq)}$), and relative low cross-linked alginate(LCA)(1wt% $CaCl_{2(aq)}$), respectively, due to the elimination of absorbed and bounded water molecules in the membrane. In case of cross-linked AdNBS-S (dNBS-S/ALG= 20/80), composite material with $CaCl_{2(aq)}$ such as relatively low-cross-linked AdNBS-S(dNBS-S/ALG=20/80) composite material(LCLAdNBS-S) (1wt% $CaCl_{2(aq)}$) and high-cross-linked AdNBS-S(dNBS-S/ALG=20/80) composite material(HCLAdNBS-S)(5wt% $CaCl_{2(aq)}$), weight loss would be increased comparing with the non-cross-linked AdNBS-S(dNBS-S/ALG=20/80) composite material sample (**Figures 4(C)**, **(F)**, and **(I)**). This increase may be due to more adsorption of water molecules present along with Ca^{2+} molecules while cross-linking with $CaCl_2$ aqueous solution. From TGA results, relatively high Tdmax(i) values of AdNBS-S composite materials were observed at 270–300°C in stage II comparing with the 250°C of non-cross-linked alginate(NCA) (**Figure 4(A)**). When the high concentration of $CaCl_2$ (5wt%) added, the relative high Tdmax(i) value of high-cross-linked alginate(HCA) was observed at ca. 270°C comparing with

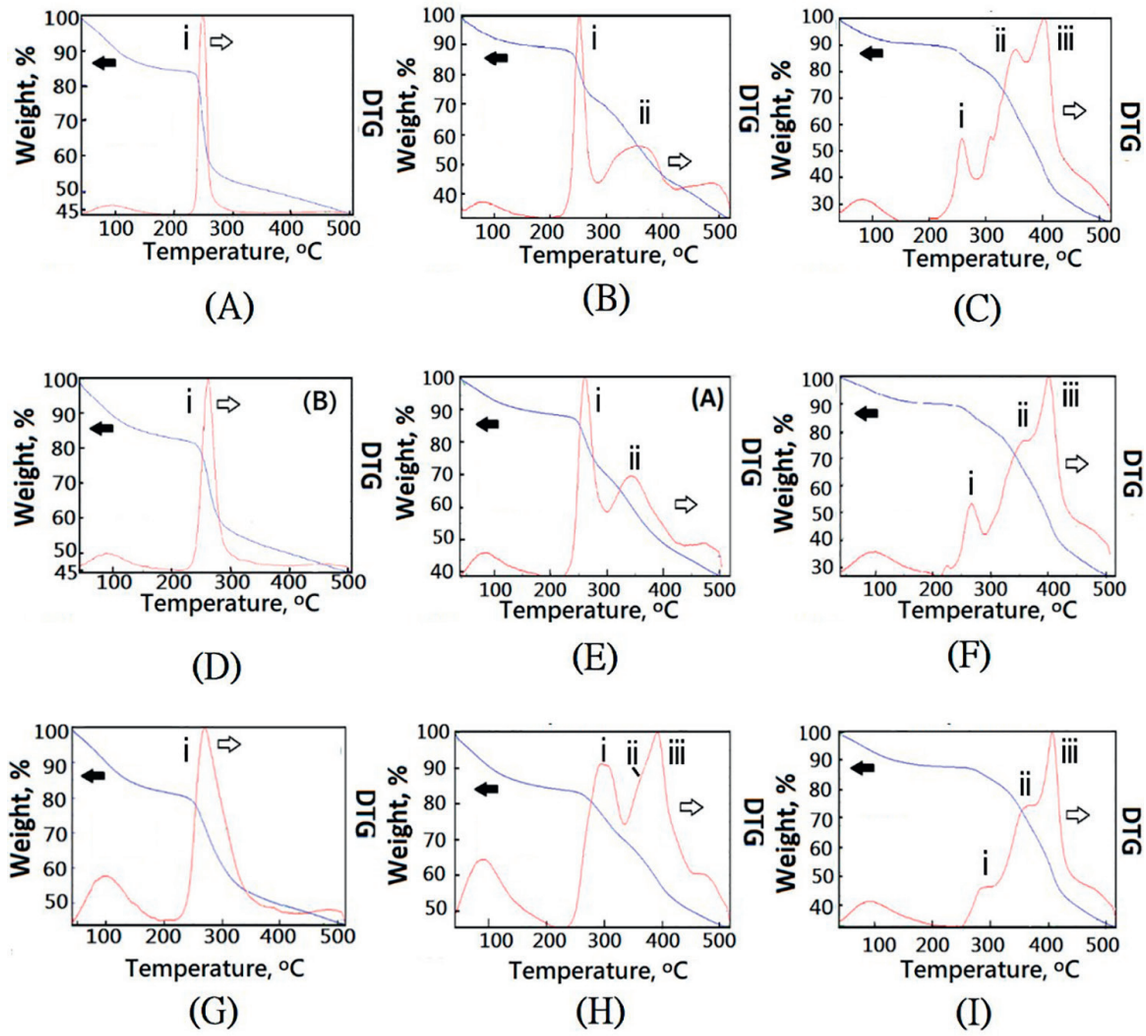

Figure 4.
Thermogravimetric analysis of the composite membranes with/without cross-linking reaction, (A) non-cross-linked alginate material (NCA); (B) non-cross-linked AdNBS-S (5/95) (NCHAdNBS-S); (C) non-cross-linked AdNBS-S (20/80) (NCLAdNBS-S); (D) relative low-cross-linked alginate(LCA) (1wt% $CaCl_{2(aq)}$; (E) relative low-cross-linked AdNBS-S (5/95) (LCHAdNBS-S) (1wt% $CaCl_{2(aq)}$); (F) relative low-cross-linked AdNBS-S (20/80) (LCLAdNBS-S) (1wt% $CaCl_{2(aq)}$); (G) high-cross-linked alginate(HCA) (5wt% $CaCl_{2(aq)}$); (H) high-cross-linked AdNBS-S (5/95)(HCHAdNBS-S) (5wt% $CaCl_{2(aq)}$); (I) high cross-linked AdNBS-S (20/80) (HCLAdNBS-S) (5wt% $CaCl_{2(aq)}$).

the 250°C of non-cross-linked alginate(NCA) and 252°C of relative low-cross-linked alginate molecule(LCA)(1wt%). Furthermore, when the high concentration of $CaCl_2$ (5wt%) was added, the relatively high Tdmax(i) values of high-cross-linked AdNBS-S such as HCHAdNBS-S and HCLAdNBS-S were observed at ca. 300°C comparing with the 270°C of high-cross-linked alginate (5wt%)(HCA) (**Figure 4(G)**). It would be due to the association between the ALG molecule and dNBS-S. Similarly, the relatively high Tdmax(ii) value of cross-linked AdNBS-S composite materials would be observed at ca.370°C. Particularly, much higher Tdmax(iii) values than Tdmax(ii) values of cross-linked AdNBS-S composite materials were observed at 400°C, which might be contributed to the formation of new mixed cross-linked network micro-structures of ALG and dNBS-S molecules.

When a little amount of dNBS-S was introduced into the AdNBS-S composite materials without $CaCl_2$, weak ionic association between –COOH group of alginate molecule and -NH_2 group of dNBS-S molecule was formed and which is difficult to

build up the cross-linking structure. With an increasing introduction of dNBS-S to AdNBS-S composite materials, ordinary ionic association between –COOH group of alginate molecule and $–NH_2$ group of dNBS-S was employed to build weak ionic cross-linking microstructure. When a large amount of dNBS-S was introduced into the AdNBS-S composite materials without $CaCl_2$(NCLAdNBS-S), strong ionic association between -COOH group of ALG molecule and $–NH_2$ group of dNBS-S was employed to build up strong ionic cross-linking microstructure.

When a little amount of dNBS-S was introduced into the dNBS-S/alginate composite membrane with 1wt% $CaCl_2$(LCHAdNBS-S), weak ionic association between –COOH group of alginate molecule and $-NH_2$ group of dNBS-S and weak ionic associations among –COOH group of alginate molecule, Ca^{2+}, and –COOH group of alginate molecule could be found. The remarkable cross-linked microstructure was difficult to be observed. Tdmax(iii) value could not be found in DTG of LCHAdNBS-S results (Figure (E)). Weak ionic association between –COOH group of alginate molecule and $–NH_2$ group of dNBS-S and weak ionic associations among –COOH group of alginate molecule, Ca^{2+}, and –COOH group of alginate molecule were employed to build weak ionic cross-linking microstructure. The overlapped Tdmax(ii,iii) values of AdNBS-S (LCHAdNBS-S) could be observed at 390°C. With an increasing introduction of dNBS-S to AdNBS-S composite materials with 5wt% $CaCl_2$, some strong ionic associations were employed to build strong mixed ionic cross-linked microstructure. The remarkable high Tdmax(iii) values of AdNBS-S could be observed at 400°C (HCLAdNBS-S). That is, when the high concentrations of $CaCl_2$(5wt%) and dNBS-S were added, some different associations would be enhanced, such as association between –COOH group of alginate molecule and $–NH_2$ group of dNBS-S, associations among –COOH group of alginate molecule, –COOH group of dNBS-S, and Ca^{2+} ion, associations among –COOH group of alginate molecule, –COOH group of alginate molecule, and Ca^{2+} ion, and associations among –COOH group of dNBS-S, –COOH group of dNBS-S, and Ca^{2+} ion.

With an increasing additions of dNBS-S to composite membranes with 1wt% $CaCl_2$, ordinary ionic association between –COOH group of alginate and $–NH_2$ group of dNBS-S was employed to build weak ionic cross-linked microstructure (**Figure 5**). When a large amount of dNBS-S was introduced into the dNBS-S/alginate composite membrane with 1wt% $CaCl_2$, some ordinary ionic associations such as ionic association between –COOH group of alginate molecule and $–NH_2$ group of dNBS-S, ionic between among –COOH group of alginate molecule, Ca^{2+}, and –COOH group of dNBS-S, and ionic between among –COOH group of dNBS-S, Ca^{2+}, and –COOH group of dNBS-S. The remarkable high Tdmax(iii) values of AdNBS-S could be observed at 400°C.

2.3 Natural soft polymeric composite materials with biomimetic 3D microarchitecture containing gelatin, alginate, and decellularized extracellular matrix via supercritical fluid treatments

For specific clinic applications, the gelatin could also be employed to prepare cross-linked porous natural soft polymeric composite materials with biomimetic 3D microarchitecture containing gelatin, alginate, and decellularized nano-bioscaffolds. A series of composite materials with a biomimetic 3D microarchitecture were prepared based on a fixed weight ratio of gelatin, alginate, and decellularized nano-bioscaffolds. An aqueous gelatin(G) solution and an aqueous alginate(A) solution (weight ratio is 2:1) were homogenized thoroughly. A mixed aqueous solution of gelatin(G) and alginate(A) was obtained as an aqueous GA solution. Briefly, the desired amount of decellularized

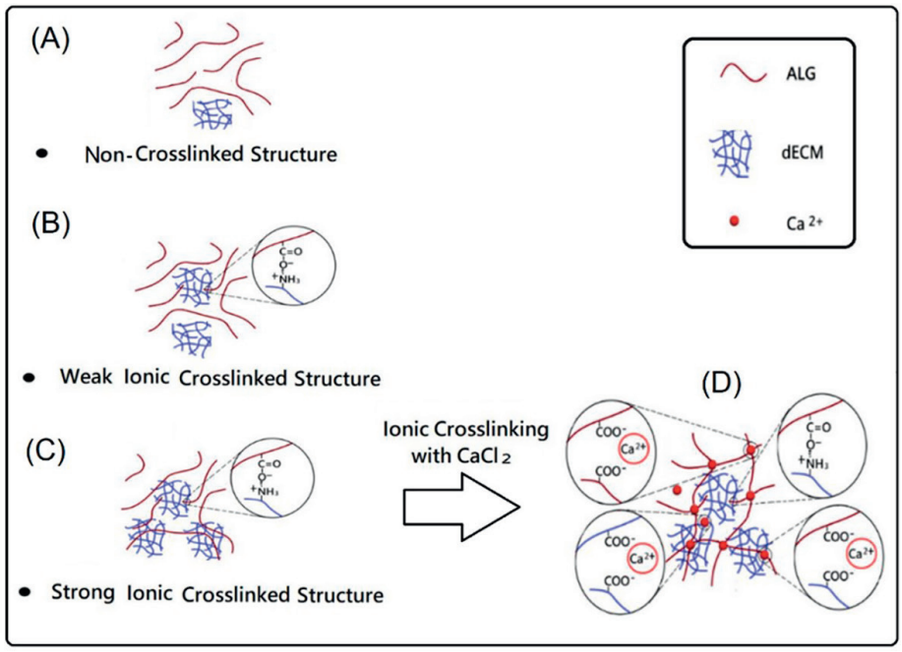

Figure 5.
Proposed model of ionic cross-linked structure from Ca^{2+} ions, alginate molecules, and dNBS-S. (A) non-cross-linked structure, (B) weak ionic cross-linked structure, (C) weak strong ionic cross-linked structure, (D) ionic cross-linked interpenetrating structure.

nano-bioscaffolds powder was first dispersed completely in water. Then, the aqueous GA solution was homogenized thoroughly with the dispersed decellularized nano-bioscaffolds solution. A mixed aqueous solution of gelatin/alginate(GA) and decellularized nano-bioscaffolds was then molded and frozen and then lyophilized. Polymeric porous natural soft polymeric composite materials(GA/dNBS) with biomimetic 3D microarchitecture containing gelatin, alginate, and decellularized nano-bioscaffolds were obtained. The resulting GA/dNBS was further soaked in $CaCl_2$ or GTA aqueous solution with various soaking times for cross-linking reaction with magnet mixer. The cross-linked GA/dNBS solutions were then frozen and dried. A series of designed cross-linked porous composite materials with biomimetic 3D microarchitecture containing gelatin, alginate, and decellularized nano-bioscaffolds could be obtained [32].

2.4 Natural soft polymeric composite materials with biomimetic 3D microarchitecture containing bovine Achilles tendon type I collagen and decellularized extracellular matrix via supercritical fluid treatments

The bovine Achilles tendon type I collagen was dispersed in an acetic acid solution and stirred to get a full dispersion collagen gel. The decellularized extracellular matrix immersed in acetic acid solution at the same concentration with collagen gel resolution was respectively placed on the table concentrator of 25 and 37°C for 24 h, allowing decellularized extracellular matrix to fully swell in acetic acid solution to obtain a decellularized extracellular matrix gel. Afterward, the decellularized extracellular matrix gels were added into the collagen gel following continuous stirring to obtain the composite hydrogel with a final ratio of 9:1 (wt/wt) of collagen and decellularized extracellular matrix. The composite gel was lyophilized. The composite nanobioscaffolds were obtained. After, those scaffolds were fully cross-linked by immersion in a 0.1% (v/v) glutaraldehyde solution (75% ethanol aqueous solution) for 1 h, freeze-dried, and

sterilized at a dose of 25 kGy. Finally, the cross-linked collagen/decellularized fibrous extracellular matrix composite nano-bioscaffolds were obtained.

3. The 3D bioprinting applications of natural soft polymeric materials with biomimetic 3D microarchitecture

3.1 Preparation of natural soft polymeric scaffolds with biomimetic 3D microarchitecture by extrusion-based bioprinting procedure with/without cells

Preparation of natural soft polymeric scaffolds with biomimetic 3D microarchitecture could be carried out from dNBS-S and ALG by using an extrusion-based bioprinting procedure with/without cells (**Figure 6**). The uncross-linked natural soft polymeric scaffolds having biomimetic 3D microarchitectures (**Figure 6(A)**) were obtained. Subsequently, the cross-linked interpenetrating composite membranes with/without cells could be obtained after ionic cross-linking procedures (**Figure 6(B)**). On the other hand, the cross-linked interpenetrating composite membranes with/without cells (**Figure 6(D)**) could be directly obtained by using a dual extrusion-based bioprinting procedure (**Figure 6(C)**). Further, introduction of gelatin in designed natural soft polymeric materials with biomimetic 3D microarchitecture could enhance structural and thermal stabilities for tissue engineering and 3D bioprinting applications as a scaffold (**Figure 7**) [32].

3.2 Design of natural soft polymeric materials with biomimetic 3D microarchitecture for dNBS-containing skin equivalents by using a layer-by-layer-dispensing method as active cell-containing wound dressings

Recently, skin grafts could be fabricated using a commercially available bioprinter(CELLINK) [33]. PLG mech was used as a mech to build up a skin construct. For medical application of skin grafts, the designed alginate-based

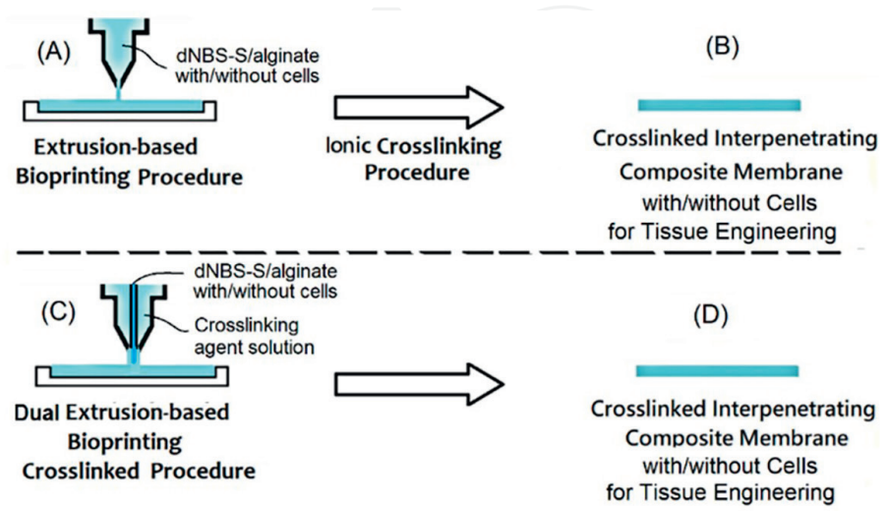

Figure 6.
Proposed model of ionic cross-linked structure from Ca^{2+} ions, alginate molecules, and dNBS-S/alginate. (A) Non-cross-linked structure, (B) weak ionic cross-linked structure, (C) weak strong ionic cross-linked structure, (D) ionic cross-linked interpenetrating structure.

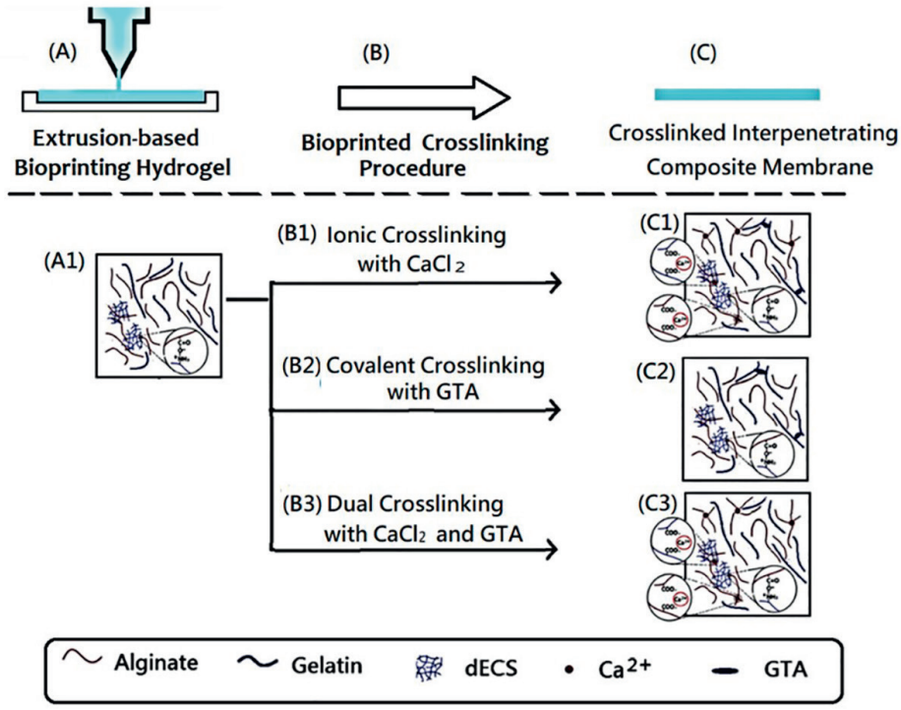

Figure 7.
Proposed model of ionic cross-linked structure from Ca^{2+} ions, alginate molecules, and dNBS-S/alginate. (A) Non-cross-linked structure, (B) weak ionic cross-linked structure, (C) weak strong ionic cross-linked structure, (D) ionic cross-linked interpenetrating structure.

biopolymeric mech containing dECM could be employed to displace PLG mech. The dECM-containing skin equivalents with a dermal layer could be designed using a layer-by-layer-dispensing method. In the concept, a designed dermal construct could be generated by dispensing dermal bioink containing human endothelial cells (ECs), fibroblasts (FBs), and pericytes (PCs) and transfer these cells such as FBs, PCs, and ECs dispensed from a syringe into a mold at an extrusion pressure. A sterile alginate-based biopolymeric mesh was added on top of the first printed dermal layer and incubated at 37°C. The alginate-based biopolymeric mesh was sterilized prior to printing by immersion in a 70% ethanol solution for 30 min and allowed to dry for 1 h at room temperature. Upon gelation, additional dermal bioink containing FBs, PCs, and ECs was printed on top of the mesh, incubated at 37°C until complete gelation, and submerged in media. The resulting construct was further submerged in a larger volume of media to prevent rapid exhaustion of nutrients. Medium was changed daily. After 4 days under medium submersion to allow self-assembly of endothelial networks, the dermal construct was carefully transferred for clinic applications such as an active cell-containing wound dressing (**Figure 8(A)** and **(B)**) or further was bioprinted an additional keratinocytes (KCs) layer to obtain an active KCs-containing wound dressings for wound management (**Figure 8(C)** and **(D)**).

3.3 Design of natural soft polymeric materials with biomimetic 3D microarchitecture for dNBS-containing skin equivalents by using a whole-dispensing method

For specific medical application of skin grafts, the dECS-containing skin equivalents with a dermal layer could be designed using a *whole*-dispensing method. In the concept,

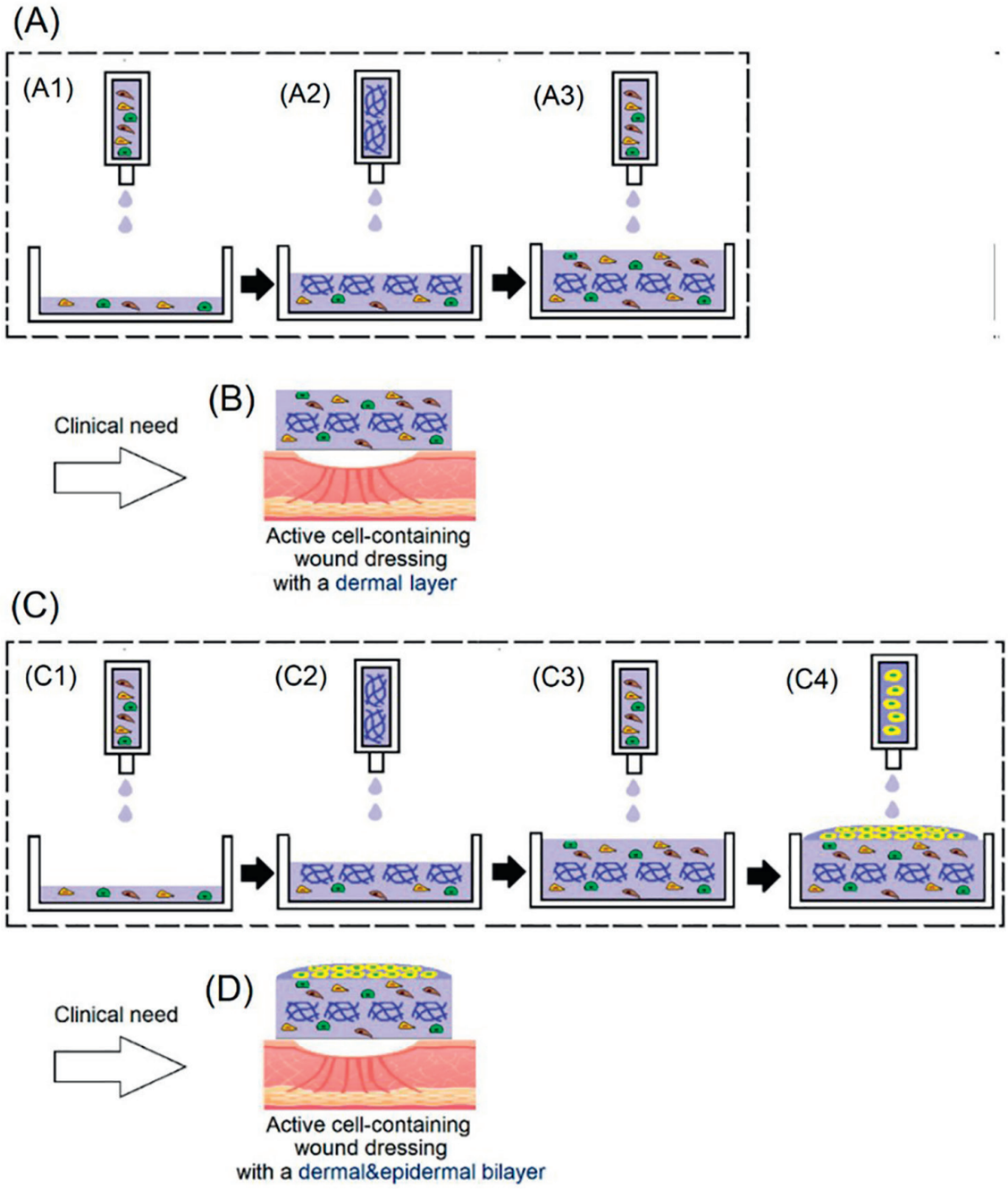

Figure 8.
Proposed model of active cell-containing and active keratinocytes-containing wound dressings for wound management. (A) preparation of an active cell-containing wound dressing, (B) clinical application of an active cell-containing wound dressing, (C) preparation of an active keratinocytes-containing wound dressing, and (D) clinical application of an active keratinocytes-containing wound dressing.

a designed dermal construct could be generated by dispensing dermal bioink containing human endothelial cells (EC), fibroblasts (FBs), pericytes (PCs) , and dECS. The dermal bioink was transferred from a syringe into a mold by using extrusion-based bioprining. A bioprinted dermal layer was obtained and incubated at 37°C (**Figure 9**). The resulting dECS-containing dermal construct was further submerged in a larger volume of media to prevent rapid exhaustion of nutrients. Medium was changed daily. After 4 days under medium submersion to allow self-assembly of endothelial networks, the dECS-containing dermal construct was carefully transferred for clinic applications such as an active dECS/cell-containing wound dressings (**Figure 9(A)**) or further

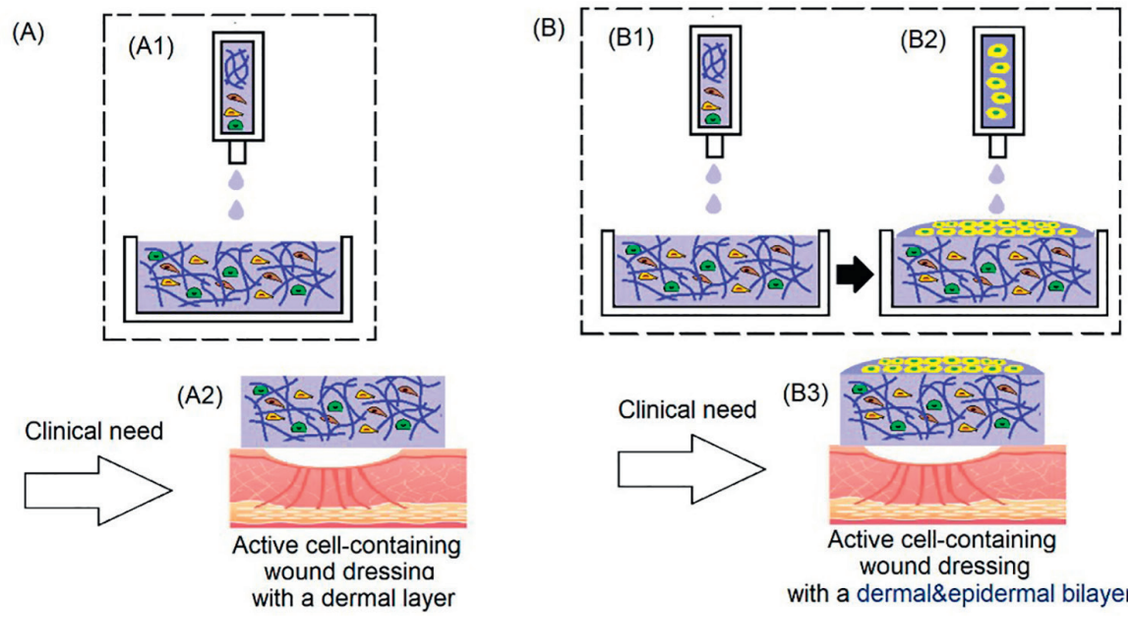

Figure 9.
Proposed model of (A) an active dECS/cell-containing wound dressings and (B) an active dECS/KCs-containing wound dressings.

was bioprinted an additional keratinocytes (KCs) layer to obtain an active dECS/KCs-containing wound dressings for wound management (**Figure 9(B)**).

4. Design of synthetic soft polymeric materials with biomimetic 3D with 3D bioinspired structural foam-wall microarchitectures

For regenerative applications, existing biomedical membranes such as collagen membranes have demonstrated the ability to promote or inhibit cell proliferation. Pure collagens suffer from uncontrollable rapid degradation and weak mechanical strength [34–37]. Generally, synthetic polymers have better mechanical properties and stability than collagen [38]. Polyvinyl alcohol(PVA), which is an FDA-approved material, was widely used in various biomedical applications, including surgical sponges, osteochondral grafts, contact lenses, artificial blood vessels, and implantable medical devices [39, 40] (e.g., bone regeneration [41], wound healing [42], and dental applications [43]) because of the desirable properties such as biocompatibility, non-degradability, low protein absorption, and easily tunable mechanical properties. PVA matrix was characterized by its super water absorbent property, great durability and cleaning ability, and its super soft texture when moist. Using sulfuric acid as catalyst and a suitable pore-forming agent, this porous PVA foam was prepared through PVA acetalization. In usual, some pore-forming agents, such as starch, surfactants, or the reagents [44, 45], which could be employed to produce gas during the cross-linking reaction to prepare PVA foam matrix. Also, water was used as a pore-forming agent to obtain porous structure without any other additional pore-forming agents [46]. Starch was a pore-forming agent that had been commonly used in the preparation of porous PVA matrix [47, 48]. The average pore diameter of PVA foam varied from 30 to 60 μm when wheat-starch was used and varied from 60 to 100 μm when potato starch was used [49, 50]. However, the volumes of PVA matrix gradually shrunk with the increasing acetalization degree and water was continuously excluded during the

acetalization process as observation. The PVA matrix with compacted or closed cell porous structure and a poor interconnectivity was obtained. The resulting PVA foam had residual pore-forming agent and undesirable degradable products, which might be harmful for biomedical applications such as tissue engineering or wound management [50]. The PVA/collagen composite materials were successfully developed in the forms of patches, nanofibers, hydrogels, polymer blend, mixed foam, and dual layers [17–55], which were mainly employed for osteochondral defects application [51], tissue-engineered corneas [52], cartilage tissue engineering [53], and wound healing [54, 55]. PVA was employed to modulate the mechanical properties, degradation properties, and cell regulation ability of PVA-based composite materials, which would show the ability to regulate the cell adhesion and proliferation behavior of cell and play a critical role in tissue regeneration [56, 57]. With a strong focus on therapeutic applications, the characteristics of composite materials for medical or regenerative applications examine the inspirations from nature [58, 59].

4.1 Design of synthetic soft polyvinyl alcohol materials with 3D bioinspired structural foam-wall microarchitectures

Biomimetic designs would bring effective materials that are sources of inspiration to biomedical engineers. For tissue engineering and medical applications, a novel bioinspired soft matrix with supporting interconnective foam-wall microarchitectures and/or struts made of cross-linked polyvinyl alcohol with air cavities inspired by avian skeleton and feather rachises was designed. The fully open-cell microstructures with air cavities, structural foam-walls, and structural pneumaticity bioinspired by avian feather rachises and pneumatic bone could be designed. The foam-wall showed a "foam-in-a-foam" microstructure and provided internal reinforcements and pneumaticity [60, 61].

Also, the corresponding foaming process was established. The bioinspired soft matrix with high interconnectivity was fabricated by using a designed air stream pore-forming process [34], which could regulate different pore sizes and microstructure of resulting materials as shown in **Figure 10**. Furthermore, the bioinspired synthetic soft polyvinyl alcohol material was employed to prepare a series of biological modified synthetic soft polyvinyl alcohol materials to provide new functional characteristics for specific clinic and regenerative applications.

The traditional designs of polyvinyl alcohol matrix were prepared by traditional starch pore-foaming process or air-assisted starch pore-foaming process. The medical drainage materials with fully open-cell microstructure could not be obtained. It is difficult to form air cavities to provide interconnectivity and structural support. To build up the stable air cavities, foam walls, and structural pneumaticity bioinspired by avian feather rachises, the introduction of clean atmospheric flow in the foaming process of polyvinyl alcohol matrix would be considered (**Figure 11**). The clean air was incorporated during the pore-foaming process and cross-linking process for formation of air cavities, foam walls, and structural pneumaticity bioinspired by avian feather rachises and pneumatic bone, which could be considered as a biomimetic airstream pore-foaming process. The clean air current was employed to avoid impurity. Complete cross-linking reaction for preparation of polyvinyl alcohol foam materials was also important. During starch-containing pore-foaming process, the pore-foaming agent, starch, could not provide enough driving force to form atmospheric flow, which would promote formation of air cavities with structural support, foam walls, and structural pneumaticity. New biomimetic design of PVA matrix with

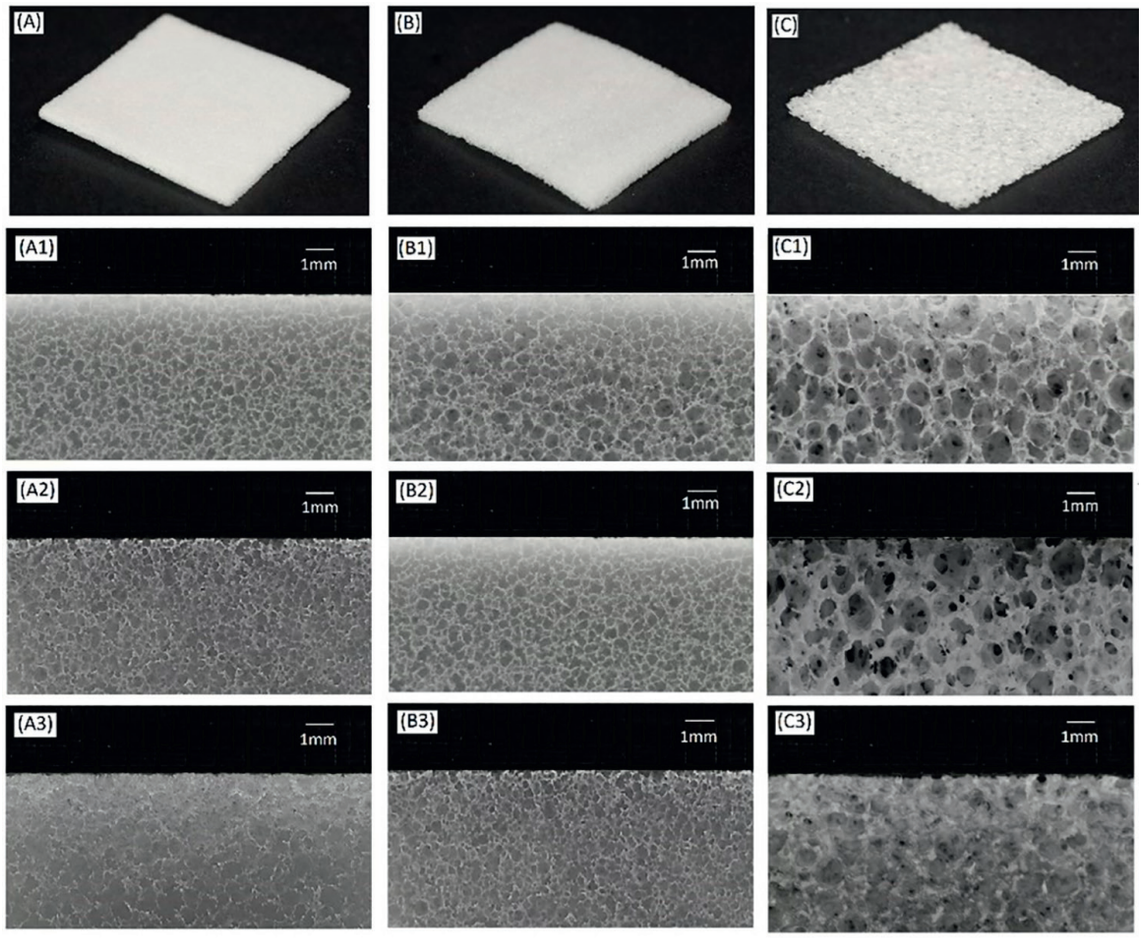

Figure 10.
Macroscopic images of designed synthetic soft polyvinyl alcohol materials with different pore sizes and microstructure. (A) Diameters were ca. 300:(A1) dried type, (A2) subhumid type, (A3) moist type; (B) Diameters were ca. 500:(B1) dried type, (B2) subhumid type,(B3) moist type; and (C) Diameters were ca. 900:(C1) dried type, (C2) subhumid type, (C3) moist type.

air cavities inspired by avian skeleton and feather rachises was prepared by using a designed air flow pore-foaming process without starch pore-foaming agent. A novel b-PVA with fully open cells and channels could be designed and prepared by using a clean airstream pore-foaming process. The reduced pressure could be employed to build up a clean airstream pore-foaming environment. Furthermore, a morphological evaluation of the resulting was carried by using SEM as shown in **Figure 6**. The resulting PVA matrix exhibited spongy structure with fully open-cell interconnecting porous network.

Porous matrices served as a guide for tissue regeneration as a three-dimensional substrate with temporary mechanical support for cell attachment, proliferation, infiltration [62]. The morphology was the key feature that affects both biological and mechanical efficiency of the medical matrices, which would be needed to provide a porous architecture with high interconnectivity to enable cell infiltration, nutrient flow, and integration of the material within the host tissue [63]. Various matrix manufacturing techniques such as emulsion templating [63], gas foaming of heterogeneous blends [64], electrospinning [65], and additive manufacturing [66] had been widely used to introduce porosity into tissue engineering scaffolds. However, PVA matrix always exhibited no interconnectivity or limited interconnectivity

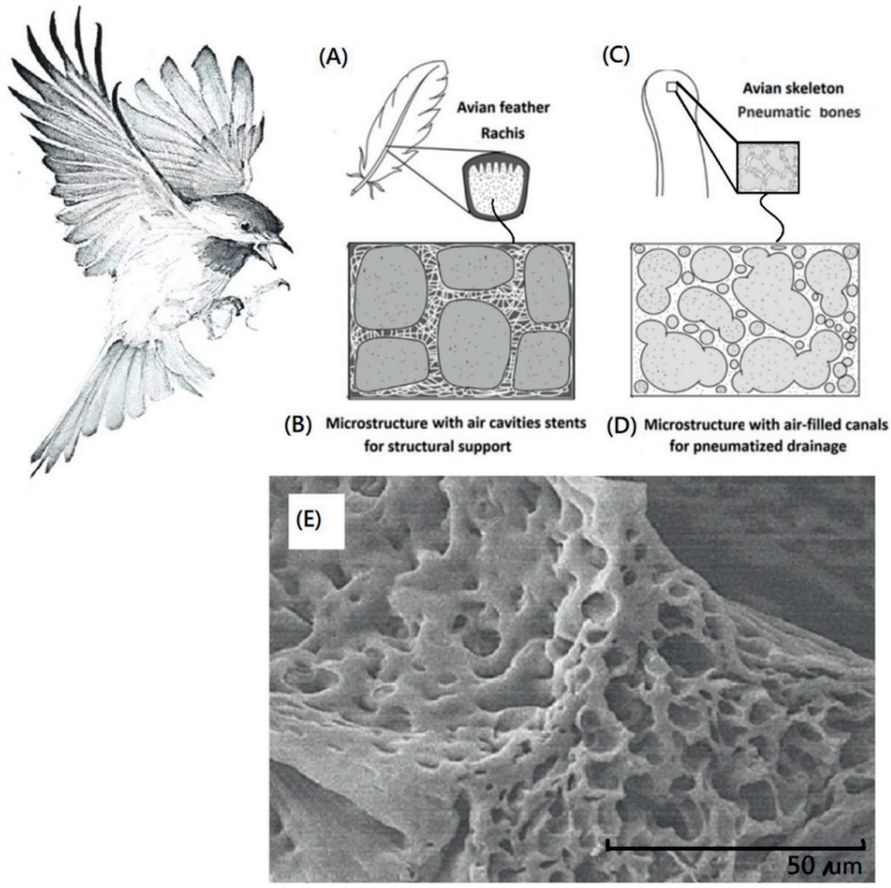

Figure 11.
Microstructures of new biomimetic design of bioinspired PVA matrix were inspired by avian skeleton and feather rachis containing foam-walls. (A) avian feather rachis, (B) microstructure with air cavities stents for structural support, (C) avian skeleton pneumatic bones, (D) microstructure with air-filled canals for pneumatized drainage, and (E) morphological evaluation of new biomimetic design of bioinspired PVA matrix by using scanning electron microscopy (SEM).

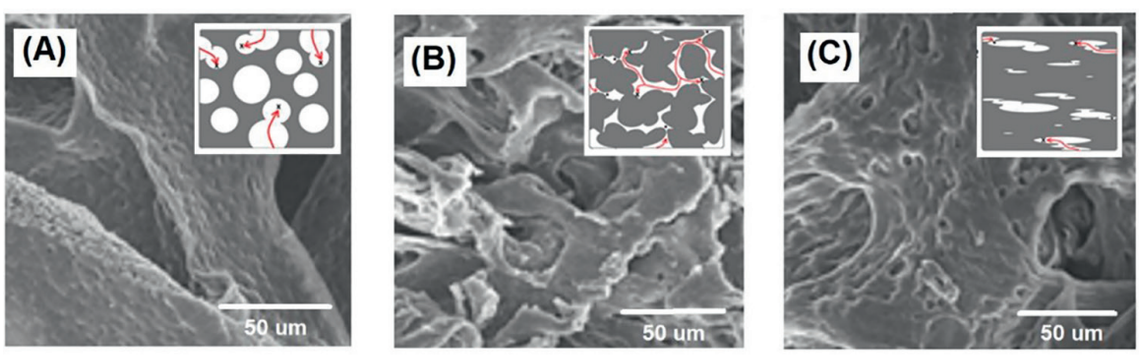

Figure 12.
The microstructural morphological evaluations of commercial soft materials with limited interconnectivity, (A) blind pore, (B) compacted pore, and (C) inaccessible pore.

because of inaccessible pore, blind pore, and compacted pore within the microstructure (**Figure 12**), which might be due to poor foaming ability by using traditional starch pore-foaming process, air-assisted traditional starch pore-foaming process, or incomplete cross-linking reaction of PVA. Biomimetic airstream pore-foaming process was employed as a new matrix fabrication technique to prepare a bioinspired

polyvinyl alcohol (b-PVA) with a foam-wall microstructure, which exhibited high porosity and high interconnectivity. The resulting high porosity and interconnectivity would enable cell migration, vascularization, and providing space for newly forming tissues to meet the requirements of specific tissue engineering applications and clinic treatments [66–68].

To understand advanced thermal stability of the synthetic soft polymeric materials with 3D bioinspired structural foam-wall microarchitectures matrix(b-PVA), the commercial medical PVA matrix was also studied by using TGA and DSC and compared with the results of b-PVA. The weight loss curves obtained from thermogravimetric analysis (TGA) could provide some information of thermal degradation such as small molecules, solvent, water, residual reagents, residual foaming agents, starch, weak structural molecules, and prepolymeric molecules, to identify the thermal structural stability. Most of commercial medical PVA matrix exhibited poor thermal stability, which might be due to the compacted and closed-cell microstructure [69]. With increasing temperature, several thermally degraded products and the weight loss of materials were observed. From TGA and DTG results of commercial medical PVA matrix, three stages of weight loss, such as stage I in 50–100°C, stage II in 100–250°C, and stage III in 250–500°C. First, weight loss of commercial medical PVA matrix in stage I at around 100°C was contributed to the loss of water molecules trapped in the hydrophilic PVA. The weight losses of stage I were observed in a range of 3–5 wt%. Second, TGA and DTG spectra of commercial medical PVA matrix in stage II exhibited slight thermal hydrolysis signals increasing with temperature, indicating that the materials might have a poor thermal stable structure and impurity. The weight losses of stage II were determined to be in a range of 2–9 wt%. The relative very low values of initial hydrolysis temperature in stage II were observed at 110–160°C, indicating the thermal degradation of the commercial medical PVA matrix would be happened easily and harm seriously for biomedical applications such as biocompatibility and tissue engineering. Third, TGA and DTG spectra of commercial medical PVA soft matrix in stage III exhibited quite broad peak of DTG curve and the relative low values of initial hydrolysis temperature in stage III were observed in a range of 220–250°C, indicating commercial medical PVA soft matrix might be incomplete cross-linked structures with poor thermal structural stability and incomplete entanglement microstructure with closed cells [34]. Differential scanning calorimeter analysis (DSC) of the commercial medical PVA matrix exhibited some peak below 100°C such as 56, 65, 68, 75, and 95°C, which might be due to the residual compounds such as unreacted PVA or starch pore-forming agents [70]. In general, the conventional method of manufacturing PVA matrix by using the pore-forming agents such as wheat starch (61.8°C [71], 56.2°C [72], and 68.2°C [73]), pea starch (59.8°C [72]), corn starch (71.2 and 80.0°C [71]), potato starch (66.6°C [71], 63.0°C [72], and 72.2°C [73]), cassava starch (65.1°C [73]), tapioca starch (69.9°C [73]), maize starch (76.7°C [73]), and rice starch (68.3°C [71] and 67.8°C/75.3°C [72]). The DSC values of the commercial medical PVA matrix observed at 84–110°C might be contributed to amylopectin part in starch. In the case of the amylopectin part in sago starch, the melting temperature peak was between 50 and 150 °C [74]. Most of the commercial products with compacted and closed cell microstructure were determined and characterized; the results might be contributed to the evident of residual starch after starch pore-foaming process, which could not provide a good support and drainage microstructure. The addition of starch and thermal depredated compounds would be harmful to the clinical applications and risks of pollution in storage system of the resulting soft medical drainage material.

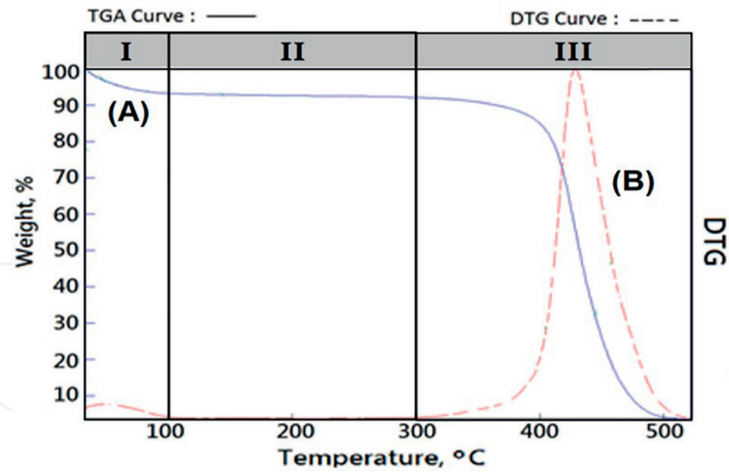

Figure 13.
Thermal characteristics of new bioinspired PVA(b-PVA) matrix, (A) TGA and (B) DTG.

Also, the residual starch would be degraded with an increasing temperature and enhance risks of treatments.

From **Figure 13**, weight loss curves obtained from thermogravimetric analysis (TGA) of biomimetic PVAF could exhibit excellent thermal structural stability and high purity. First, TGA and DTG curves of bioinspired PVA matrix in the region with the temperature lower than 100°C exhibited 6wt% of weight loss, which would be due to only water molecules escaping from the materials and a good water-absorption property. Also, DSC curve of bioinspired PVA matrix was employed to identify thermal stability and exhibited a smooth signal below 100°C, which was contributed to escaping water molecules. Second, TGA and DTG curves of bioinspired PVA matrix in the region with a temperature range between 100 and 300°C exhibited no change of thermal signals, indicating high purity of synthetic soft materials. Third, TGA and DTG curves of bioinspired PVA matrix in the region with the temperature higher than 300°C exhibited a high Tdmax value >425°C and a narrow peak of DTG curve, which indicated high thermal and structural stability and a fully cross-linked structure (**Figure 13**).

A novel bioinspired soft matrix derived from PVA was designed and prepared. Fourier-transform infrared spectra of the designed synthetic soft polymeric materials with 3D bioinspired structural foam-wall microarchitectures (b-PVA) were determined. The main bands of pure PVA at 3500–3400, 2917, 1425, 1324, and 839 cm^{-1} were assigned to the O-H stretching vibration of the hydroxy group, CH_2 asymmetric stretching vibration, C-H bending vibration of CH_2, C-H deformation vibration, and C-C stretching vibration by using FTIR. After the biomimetic airstream pore-foaming process, the molecular structure of PVA matrix was also characterized. The bands at 3500–3400cm^{-1} were weakened and shifted toward higher frequencies due to the consumption of -OH (due to condensation reaction be acetalization tween PVA and formaldehyde) and the corresponding cleavage of the intra- and intermolecular hydrogen bonding. The new bands at 2952, 2913, 2861, and 2675 cm−1 ascribed to symmetric stretching vibrations of the alkyl CH_2 group, the new bands at 1239, 1172, 1129, and 1065 cm^{-1} ascribed to the stretching vibration of C-O in C-O-H groups, and a new peak at 1008 cm^{-1} ascribed to -C-O-C-O-C- stretching vibrations could confirm the formation of a formal structure of b-PVA [75, 76]. Starch of corn, cassava, and potato showed similar absorption bands below 1200 cm^{-1} [77, 78]. A absorbance band around 1150 cm^{-1},

bands at 1080 and 1020 cm^{-1}, and bands around 700–900 cm^{-1} were contributed to vibrations of the glycosidic C–O–C bond [34, 76], the anhydroglucose ring O–C stretch [34, 77], and C-O-C ring vibration [34, 76], respectively [34, 76, 77]. The absorbance band at 924 cm^{-1} was assigned to vibrational modes of a skeletal glycoside bonds of starches [34, 77]. FTIR spectrum of commercial medical PVA matrix showed the similar absorbance band at 924 cm^{-1}. However, the absorbance band at 924 cm^{-1} could not be observed in the FTIR spectra of new bioinspired PVA matrix. The absorbance band at 924 cm^{-1} might be an important evident for starch pore-foaming process and an evaluation for a structural support cell microstructure. The fingerprint region at wavenumbers 1200–600 cm^{-1} could be employed to identify the purity and molecular structure of suitable medical soft matrix. That is, the fingerprint region of new biomimetic design of medical soft matrix could identify the biomimetic super-clean airstream pore-foaming process different from those of traditional starch pore-foaming process. The residual starch pore-foaming agents were degraded easily with an increasing temperature, which might be harmful to the cleanliness of the medical soft matrix and enhance risks of pollution in biomedical application such as tissue engineering or wound management [79, 80].

For the therapeutic application of liver, bioartificial liver support system has been proposed to support the regeneration of the patient's liver [81, 82]. The PVA matrix might be considered as a suitable material. The b-PVA was a nontoxic material with favorable mechanical properties, chemical stability, and good cell adhesion, which could be easily processed and has a special three-dimensional porous structure [83, 84]. Fabrication of porous matrix as potential hepatocyte carriers for bioartificial liver support had been widely explored [85, 86]. Previous studies have tried to immobilize protein with biomaterials by using covalent binding for HepG2 cell culture [85, 86]. The designed b-PVA matrix showed a microstructure containing foam-walls with good structural support and interconnectivity, which might act as a feasible material for artificial liver devices because of biocompatibility, pore-foaming, and mechanical property [85, 86].

The human hepatoblastoma HepG2 cells could be employed for evaluation of liver therapeutic application by using an extrusion-based bioprinting procedure as shown in **Figure 14A**). The ability of cells to adhere and proliferate on the bioinspired polyvinyl alcohol (b-PVA) matrix was an important indicator for evaluating the in vivo application potential. The SEM images were used to evaluate the cell morphology on the bioinspired polyvinyl alcohol matrix after various times of human hepatoblastoma HepG2 cell culture such as 72 h as shown in **Figure 15**. After 72 h of culturing, HepG2 cells would be adhered to the scaffold and grew cover on the interface and inside of the open-cell pores. The foam-walls might provide a rough surface for HepG2 cell proliferation. The interconnected microporous microstructure of the matrix might well supports the penetration of HepG2 cells.

4.2 Design of biological modified b-PVA with 3D bioinspired structural foam-wall microarchitectures

The designed bioinspired PVA(b-PVA) was employed to form a relative biocompatible surface of a collagen-modified b-PVA, which might provide more suitable characteristics for cell adhesion and growth. Some domains in collagen molecules, such as Phe-Hyp-Gly segment, could act as ligands for the integrin family

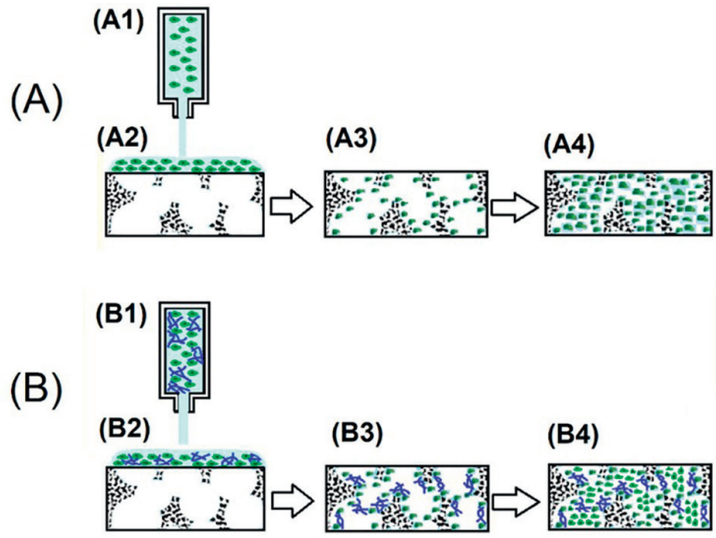

Figure 14.
Bioprinting applications of novel active liver-repairing membranes derived from synthetic soft polymeric materials with biomimetic 3D microarchitecture. (A) Active liver tissue-repairing membranes and (B) active dNBS-containing liver tissue-repairing membranes.

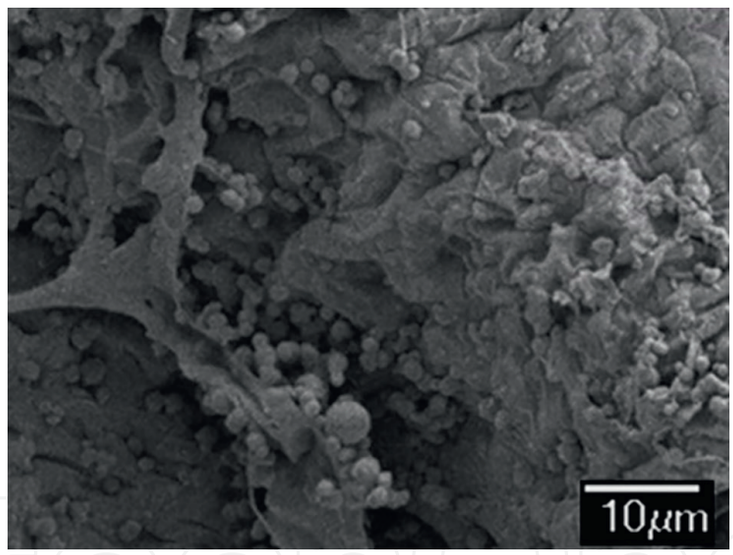

Figure 15.
SEM photographs of HepG2 cells grew on the b-PVA after 72 h (scale bar x10 μm).

receptors of cell surface and potentially activate specific biological signals to promote cell attachment and proliferation. The fully open cell and open foam-wall microstructure of b-PVA was maintained after preparation of collagen-modified b-PVA (**Figure 16**). The b-PVA and bovine Achilles tendon type I collagen were employed to prepare a bioinspired bovine Achilles tendon type I collagen-modified b-PVA composite matrix with open-cell foam-wall microarchitectures. The hydrophilic hydroxyl group within b-PVA molecules might provide a good binding with the coated bovine Achilles tendon type I collagen molecules by using hydrogen bonding and Van der Waals forces [87, 88]. Similar behavior was observed by Zhou et al. [89]. The interaction between b-PVA and bovine Achilles tendon type I collagen molecules within collagen-modified b-PVA was based on non-covalent interactions such as hydrogen

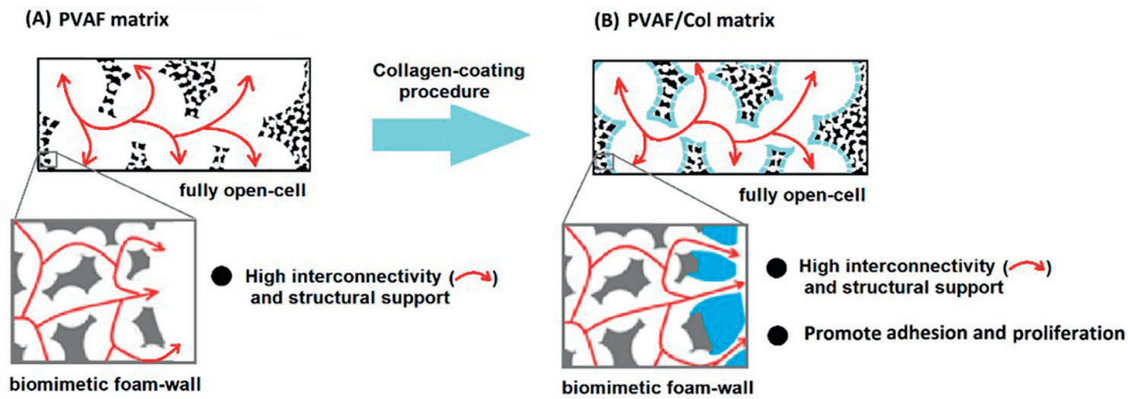

Figure 16.
Interconnected microporous microstructure of medical drainage materials, (A) the original bioinspired PVA matrix and (B) the bioinspired collagen-modified PVA composite matrix.

bonding and Van der Waals forces. The hydrogen bonding would be the main force between PVA and collagen interactions, in which collagen molecule might act as a hydrogen donor and forms hydrogen bonds with the hydroxyl group of b-PVA [90]. The bioinspired soft matrix combined the structural properties of the synthetic PVA matrix with the high cell affinity of the type I collagen, thus enhancing the matrix cytocompatibility. Collagen was the dominant component of the extracellular matrix and had been widely used in tissue engineering due to its low antigenicity, good biocompatibility, biodegradability, and nontoxicity [91]. The FTIR analysis was employed to confirm changes of molecular structure after the surface modification on the PVA matrix with collagen molecules. The absorbances at ~3300, ~2930, ~1636, ~1571, and ~1150 cm^{-1} were observed and characterized for amide A (N-H stretching), amide B(the asymmetrical stretching of CH_2 vibration), amide I(hydrogen bonding between N-H stretching and C=O), amide II(N-H bending and C-N stretching), and amide III(C-N bending, and N-H stretching), respectively. Remarkably, the collagen-modified bioinspired PVA composite matrix showed quite different absorbance from original bioinspired PVA matrix in the region of 1200–1800 cm^{-1}. After the biological surface modification on the b-PVA with collagen molecules, the resulting biological collagen-modified b-PVA still sustained a favorable biomimetic interconnected porous structure.

The morphology of the bioinspired collagen-modified b-PVA with high interconnectivity was investigated and confirmed. After 72 h of culturing, HepG2 cells were remarkably adhered to the bioinspired collagen-modified b-PVA and grew cover on the interface and inside of the open-cell porous microstructure. The SEM images intuitively displayed the growth and distribution of cells on the resulting bioinspired and collagen-modified b-PVA. HepG2 cells adhering to the type I collagen-modified b-PVA showed filopodia, which indicated that human hepatoblastoma HepG2 cells on type I collagen-modified b-PVA in a relative better proliferative condition than pure b-PVA. The stable adhesion and complete spreading could be observed in **Figure 17**. Majhy et al. reported that facile surface modification of substrate could enhance the cell-substrate interaction from a non-adherent state for promoting cell culture [62, 92]. The HepG2 cells attached and grew in cluster on the bioinspired and collagen-modified b-PVA, which was quite different from original b-PVA. The bioinspired and collagen-modified b-PVA was conductive to HepG2 proliferation, migration, expression, and functionality maintenance.

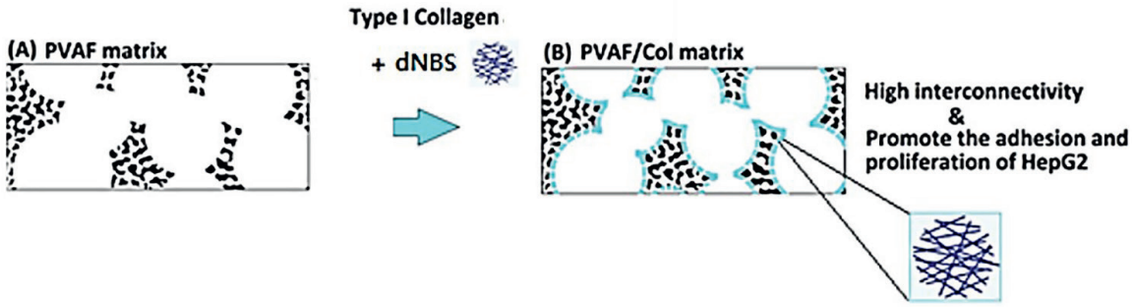

Figure 17.
Design of (A) bioinspired PVA composite matrix and the corresponding (B) dNBS-modified biological bioinspired PVA composite matrix.

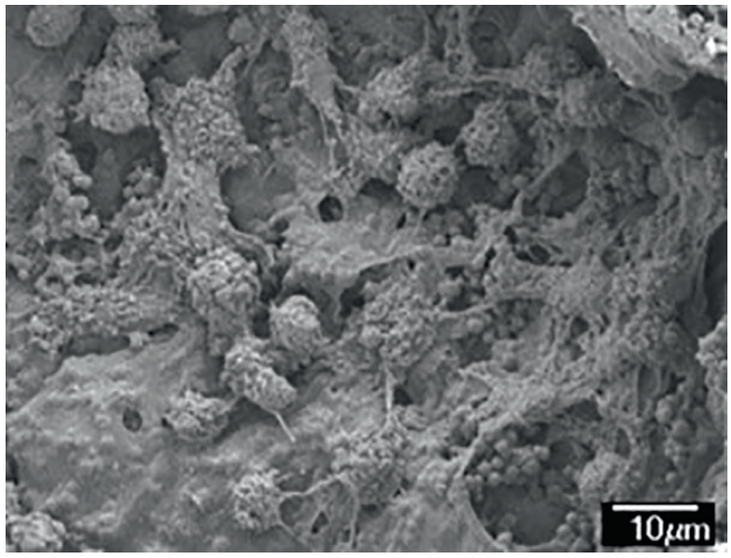

Figure 18.
SEM photographs of HepG2 cells grew on the collagen modified b-PVA (scale bar x10 μm).

HepG2 cells proliferated actively and formed cell clusters more efficiently in the collagen-modified b-PVA than original b-PVA (**Figure 18**). The collagen of collagen-modified b-PVA appeared to promote the growth and differentiation of the HepG2 cells. As shown in **Figure 18**, after 72 h, cells attached and grew well on the collagen-modified PVA composite matrix and a large number of pseudopods could be seen. The HepG2 cells would be evenly distributed on the surface of the pore of the b-PVA. Similarly, Moscato et al. reported that poly(vinyl alcohol)/gelatin hydrogels were good for growth of HepG2 cells [63, 93]. In the future, the bioinspired and collagen-modified b-PVA might serve as a promising liver cell culture carrier to be used in the biological artificial liver reactor. Both the type I collagen-modified b-PVA and the corresponding b-PVA could be considered as good materials for different tissue engineering applications. Furthermore, the type I collagen could be combined with dNBS to prepare new designed collagen/dNBS-modified b-PVA, which might provide additional 3D microenvironments within porous structure for cell adhesion and growth as shown in **Figure 17**. Also, the human hepatoblastoma HepG2 cells could be employed for evaluation of liver therapeutic application such as active liver-tissue-repairing membranes by using an extrusion-based bioprinting procedure as shown in **Figure 14(B)**.

4.3 Design of synthetic chitosan oligosaccharides-modified PVA composite matrix(COS/b-PVA) with 3D bioinspired structural foam-wall microarchitectures

Chitosan oligosaccharide (COS) is a biomaterial obtained by chemical or enzymatic degradation of chitosan derived from shrimp and crab shells [94]. The resulting chitosan oligosaccharide(COS) is composed of 2–10 glucosamines linked by β-1, 4 glycosidic bonds and the molecular weight is up to 3900 Da. The b-PVA was soaked in chitosan oligosaccharide (COS) solution and then frozen-dried. Synthetic chitosan oligosaccharides-modified b-PVA composite matrix(COS/b-PVA) with 3D bioinspired structural foam-wall microarchitectures was obtained. The open-cell microstructures were retained in chitosan oligosaccharides-modified polyvinyl alcohol(COS/b-PVA) (**Figure 19**). The connecting holes and the corresponding open channels were fully covered and filled with chitosan oligosaccharides, which provide a controlled release system of active chitosan oligosaccharide molecules for wound managements. The water permeability of the resulting chitosan oligosaccharide-modified COS/b-PVA dressings was determined by ASTM D4491 standard test methods. The good water permeability was observed in a relative higher level than 80%, which would be contributed to specific clinic applications [94–96].

4.4 Design of soft polymeric materials with 3D bioinspired structural foam-wall microarchitectures using a mixed foaming procedure combined synthetic polyvinyl alcohol with natural chitosan

A new form of polymer blend, macroporous chitosan/poly(vinyl alcohol) (PVA) foams made by a starch expansion process, exhibits the functionalities of chitosan while avoiding its poor mechanical properties and chemical instabilities. The appropriate conditions for foaming are discussed using both insoluble and water-soluble chitosan. Both insoluble/PVA and water-soluble chitosan/PVA foams demonstrated interconnected and open-cell structures with large pore size from tens to hundreds of micrometers and high porosities from 73.6 to 84.3%. The chitosan/PVA with high interconnected and open-cell structures might have potential in the tissue

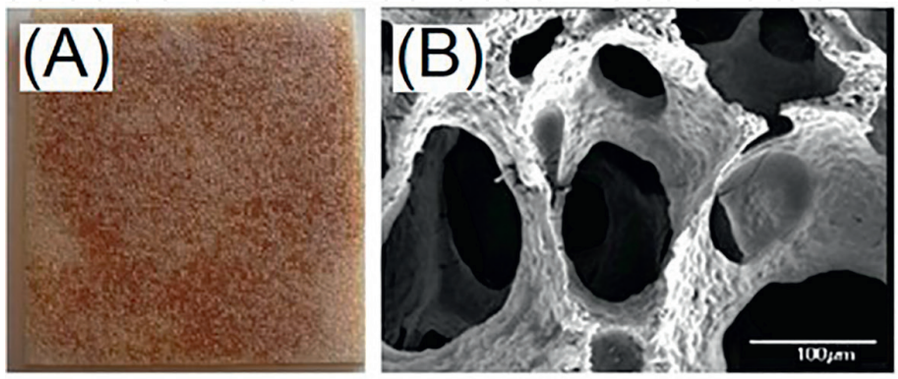

Figure 19.
(A) Photo of the designed permeable chitosan oligosaccharide modified polyvinyl alcohol complex foam (COS/b-PVA) and (B) morphology of designed chitosan oligosaccharide modified polyvinyl alcohol complex foam (COS/b-PVA) dressing with fully open-cell and open-channel microstructures.

Figure 20.
Active tissue-repairing sponges made from chitosan/poly(vinyl alcohol) (Supported by Cenefom and PARSD).

engineering and bioprinting applications [97]. The clean airstream pore-foaming process for b-PVA could be employed to build up a blend-foaming process for preparation of chitosan/poly(vinyl alcohol) (b-PVA). The chitosan/poly(vinyl alcohol) (PVA) was obtained and applied for clinic treatments such as active tissue-repairing sponges (**Figure 20**).

5. Clinic application of active tissue-repairing membranes by using 3D bioprinting and cells culture procedure

New biomimetic biomedical inventive design-thinking methods could be established for design of new clinic application such as active tissue-repairing membranes by using 3D bioprinting and cells culture procedure [98].

5.1 Clinic application of synthetic soft active tissue-repairing membranes by using 3D bioprinting and cells culture procedure

The collagen-coating PVA could be employed as a 3D-bioprinting supporting scaffold for 3D bioprinting applications of a tissue-repairing membrane such as active skin-tissue-repairing membranes and liver-repairing membranes.

The collagen-coating b-PVA could be cultured HepG2 cell to design a liver-repairing membrane as shown in **Figure 15**. Also, the bioprinting of a human skin substitute containing xeno-free cultured human EC, FBs, and PCs in a xeno-free bioink (**Figure 21(A)(A1)**) containing human collagen type I and fibronectin layered in a biocompatible collagen-coating b-PVA supporting scaffold (**Figure 21(A)(A2)**). After cells of EC, FBs, and PCs being cultured and transferred into the biocompatible collagen-coating b-PVA supporting scaffold (**Figure 21(A)(A3)**), a designed active skin-tissue-repairing membranes containing human EC, FBs, and PCs could be obtained for clinical treatments (**Figure 21(A)(A4)**). Furthermore, dNBS could be introduced into the bioink (**Figure 21(B)(B1)**) containing EC, FBs, PCs, and dNBS, human collagen type I, and fibronectin and layered in a biocompatible

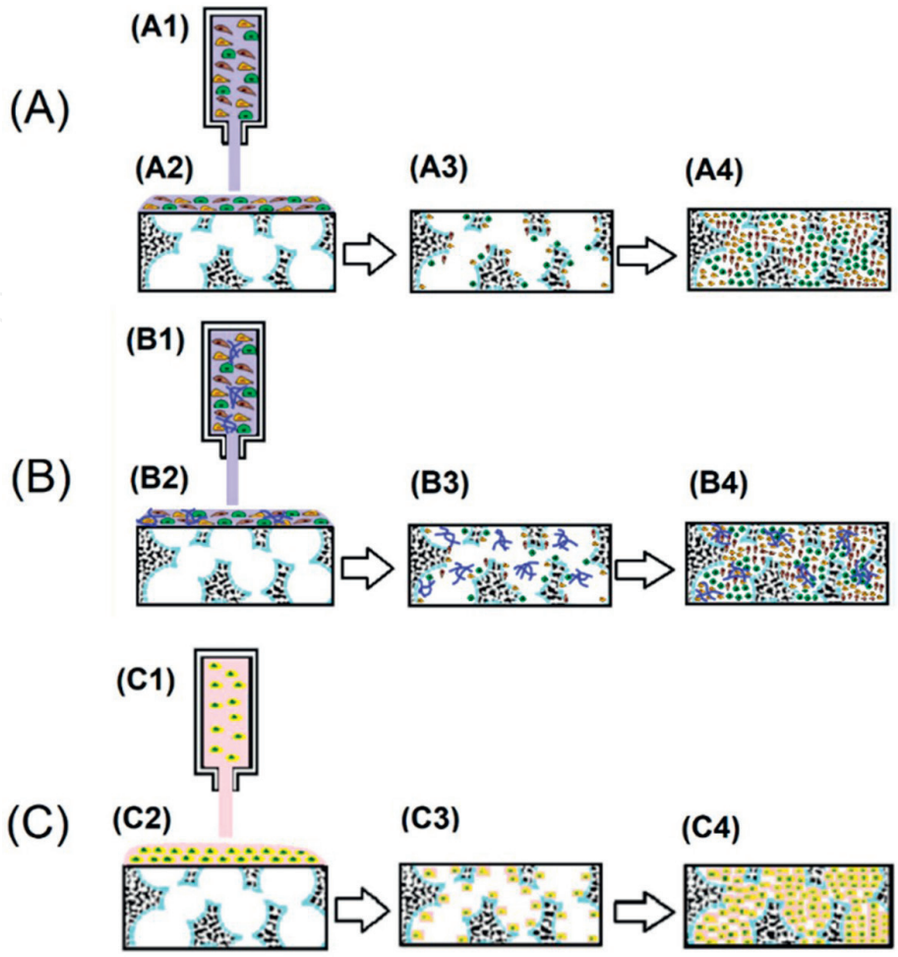

Figure 21.
Bioprinting applications of novel active skin-repairing membranes derived from natural and synthetic soft polymeric materials with biomimetic 3D microarchitecture. (A) active skin dermal tissue-repairing membranes, (B) active dNBS-containing skin dermal tissue-repairing membranes, and (C) active skin epidermal tissue-repairing membranes.

collagen-coating b-PVA supporting scaffold (**Figure 20(B)(B2)**). The collagen-coating b-PVA could be cultured EC, FBs, and PCs with dNBS (**Figure 20(B)(B3)**) to obtain a novel active dNBS-containing skin-tissue-repairing membranes containing human EC, FBs, PCs, and dNBS (**Figure 21(B)(B4)**). Independently, human KCs were introduced into a xeno-free bioink (**Figure 21(C)(C1)**). Furthermore, the collagen-coated PVA could be bioprinted with the resulting KCs bioinks (**Figure 20(C)(C2)**) and cultured with xeno-free human KCs (**Figure 21(C)**(C3)) to form active epidermal tissue-repairing membranes for clinic application in wound management (**Figure 21(C)(C4)**).

For the clinic applications, the novel active skin dermal tissue-repairing membranes, dNBS-containing active skin dermal tissue-repairing membranes, and active skin epidermal tissue-repairing membranes could be applied directly on the target wounds for different repairing steps such as dermal repairing (**Figures 22(A)** and **23(A)**) and subsequently epidermal repairing (**Figures 22(C)** and **23(C)**). Also, the additional PBS or saline could be employed to transfer the cells within the wound dressings onto the surface of wound depending on the clinic needs for different repairing steps such as dermal repairing (**Figures 22(B)** and **23(B)** and subsequently epidermal repairing (**Figures 22(D)** and **23D)**). The dNBS-containing active skin repairing wound dressings could provide a natural biomimetic 3D microarchitecture

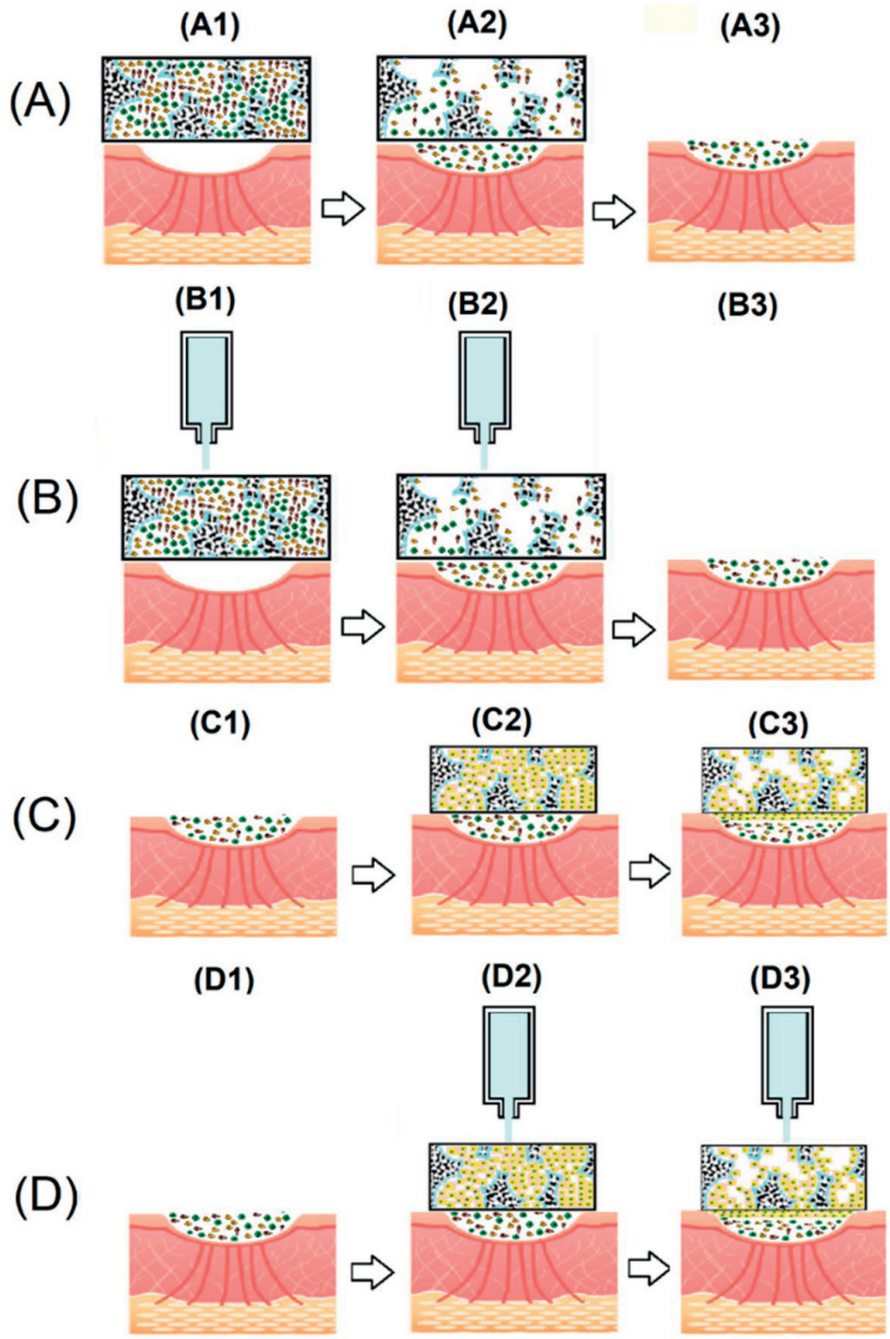

Figure 22.
Novel active skin-repairing membranes derived from synthetics oft polymeric materials with biomimetic 3D microarchitecture for wound managements. (A) Active skin dermal tissue-repairing membranes without transferring assistances, (B) active skin dermal tissue-repairing membranes with transferring assistances, (C) active skin epidermal tissue-repairing membranes without transferring assistances, and (D) active skin epidermal tissue-repairing membranes with transferring assistances.

for promotion of cell growth. The collagen-coating PVA matrix was considered as a good cell carrier for cell culturing and transferring.

6. Conclusions

Design and characterization of natural and synthetic soft polymeric materials with biomimetic 3D microarchitecture were considered. The natural soft polymeric

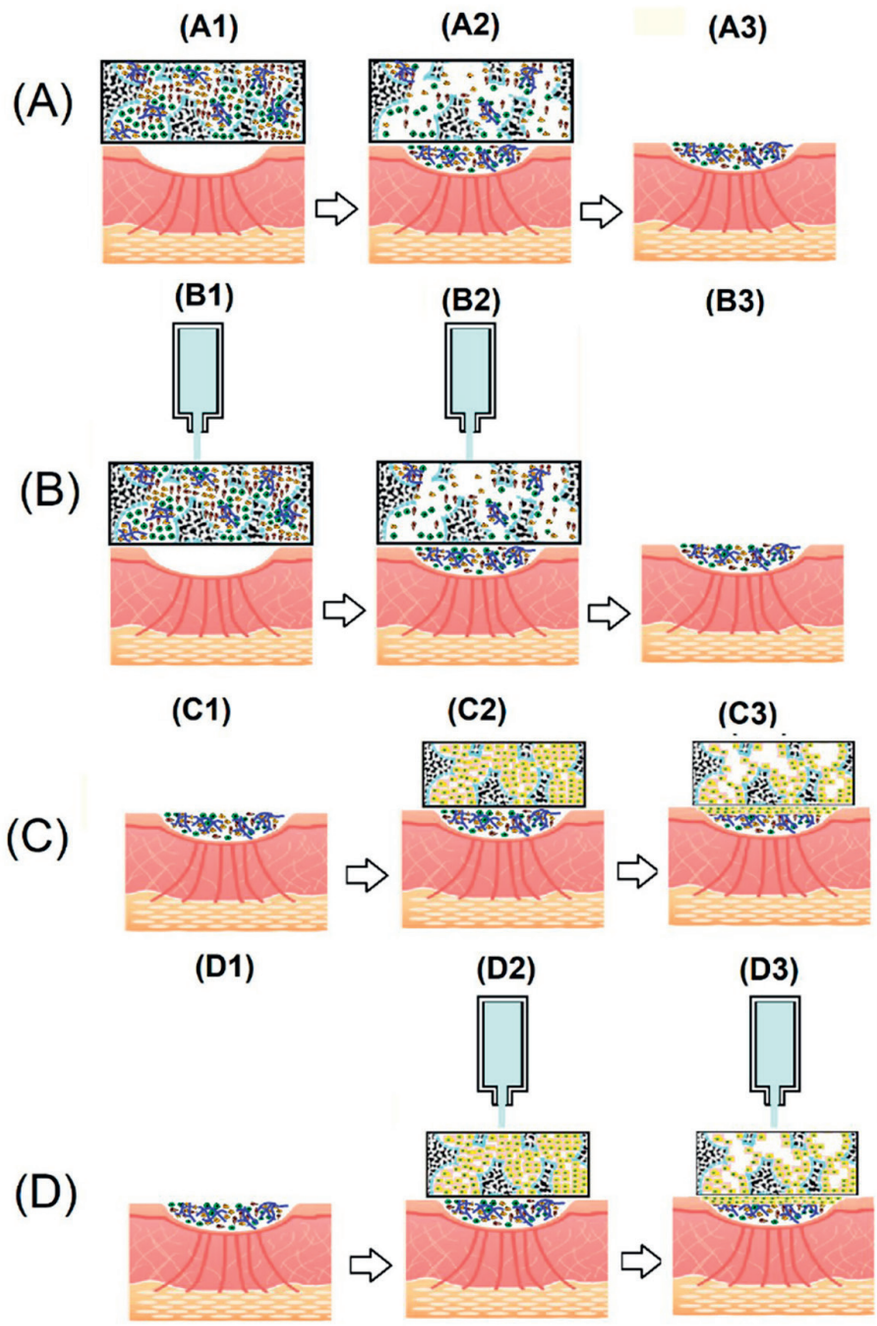

Figure 23.
Novel active dNBS-containing skin-repairing membranes derived from synthetic soft polymeric materials with biomimetic 3D microarchitecture for wound managements. (A) active dNBS-containing skin dermal tissue-repairing membranes without transferring assistances, (B) active dNBS-containing skin dermal tissue-repairing membranes with transferring assistances, (C) active dNBS-containing skin epidermal tissue-repairing membranes without transferring assistances, and (D) active dNBS-containing skin epidermal tissue-repairing membranes with transferring assistances.

materials would focus on new design bioinspired membranes containing supercritical fluids-decellularized dermal scaffolds for 3D bioprinting potential applications. Synthetic soft polymeric materials would focus on b-PVA with structural foam-wall microarchitectures. The b-PVA was designed, prepared, and showed relative higher interconnectivity than commercial medical soft matrix, which could be considered as a good potential scaffold for tissue engineering. Furthermore, the b-PVA was employed to prepare a highly biocompatible collagen-modified b-PVA composite

matrix after surface modification with type I collagen. In the future, the collagen-modified b-PVA composite matrix might serve as a promising liver cell culture carrier to be employed in the biological artificial liver reactor.

Acknowledgements

Author would like to acknowledge the Taiwan PARSD Pharmaceutical Technology Consultants Ltd. Company for financial and technical support. Additionally, the author would like to thank Gui-Feng Zhang and Yuguang Du for their technical assistance from the State Key Laboratory of Biochemical Engineering, Institute of Process Engineering, and Chinese Academy of Sciences, Beijing.

Conflicts of interest

The authors declare no conflict of interest.

Author details

Ching-Cheng Huang[1,2*] and Masashi Shiotsuki[3]

1 Department of Biomedical Engineering, Ming-Chuan University, Taiwan

2 PARSD Biomedical Material Research Center, Taiwan

3 Faculty of Science and Engineering, Tokyo City University, Japan

*Address all correspondence to: jcchuang.mcu@gmail.com

IntechOpen

© 2022 The Author(s). Licensee IntechOpen. This chapter is distributed under the terms of the Creative Commons Attribution License (http://creativecommons.org/licenses/by/3.0), which permits unrestricted use, distribution, and reproduction in any medium, provided the original work is properly cited. (cc) BY

References

[1] Murphy CA, Costa JB, Silva-Correia J, Oliveira JM, Reis RL, Collins MN. Biopolymers and polymers in the search of alternative treatments for meniscal regeneration: State of the art and future trends. Applied Materials Today. 2018;**12**:51-71

[2] Kwon H, Brown WE, Lee CA. Surgical and tissue engineering strategies for articular cartilage and meniscus repair. Nature Reviews Rheumatology. 2019;**15**(9):550-570

[3] Bilgen B, Jayasuriya CT, Owens BD. Current concepts in Meniscus Tissue engineering and repair. Advanced Healthcare Materials. 2018;**7**(11):1701407

[4] Rongen JJ, van Tienen TG, van Bochove B, Grijpma DW, Buma P. Biomaterials in search of a meniscus substitute. Biomaterials. 2014;**35**(11):3527-3540

[5] Deo KA, Singh KA, Peak CW, Alge DL, Gaharwar AK. Bioprinting 101: Design, fabrication, and evaluation of Cell-Laden 3D Bioprinted Scaffolds. Tissue Engineering. Part A. 2020;**26**(5-6):318-338

[6] Murphy SV, Atala A. 3D bioprinting of tissues and organs. Nature Biotechnology. 2014;**32**(8):773-785

[7] Filardo G, Petretta M, Cavallo C. Patient-specific meniscus prototype based on 3D bioprinting of human cell-laden scaffold. Bone Joint Research. 2019;**8**(2):101-106

[8] Cengiz IF, Pitikakis M, Cesario L. Building the basis for patient-specific meniscal scaffolds: From human knee MRI to fabrication of 3D printed scaffolds. Bioprinting. 2016;**1-2**:1-10

[9] Mishra A, Srivastava V. Biomaterials and 3D printing techniques used in the medical field. Journal of Medical Engineering & Technology. 2021;**5**(4):290-302

[10] Zhang J, Wehrle E, Rubert M, Müller R. 3D bioprinting of human tissues: Biofabrication, Bioinks, and Bioreactors. International Journal of Molecular Sciences. 2021;**22**(8):3971

[11] Ravnic DJ, Leberfinger AN, Koduru SV, Hospodiuk M, Moncal KK, Datta P, et al. Transplantation of bioprinted tissues and organs: Technical and clinical challenges and future perspectives. Annals of Surgery. 2017;**266**(1):48-58

[12] Li J, Chen M, Fan X, Zhou H. Recent advances in bioprinting techniques: Approaches, applications and future prospects. Journal of Translational Medicine. 2016;**14**:271

[13] Chen H, Zhang Y, Zhang L. Applications of bioinspired approaches and challenges in medical devices. Bio-des. Manufacturing. 2021;**4**:146-148

[14] Li Z, Huang S, Liu Y, Yao B, Hu T, Shi H, et al. Tuning alginate-gelatin bioink properties by varying solvent and their impact on stem cell behavior. Scientific Reports. 2018;**8**:8020

[15] Brovold M, Almeida JI, Pla-Palacín I, Sainz-Arnal P, Sánchez-Romero N, Rivas JJ, et al. Naturally-derived biomaterials for tissue engineering applications. Advances in Experimental Medicine and Biology. 2018;**1077**:421-449

[16] Carpio BM, Dabaghi M, Ungureanu J, Kolb MR, Hirota JA, Moran-Mirabal JM. 3D bioprinting strategies, challenges, and opportunities to model the lung tissue

microenvironment and its function. Frontiers in Bioengineering and Biotechnology. 2021;**9**:773511

[17] Huang CC, Chen YJ, Liu HW. Characterization of composite nano-bioscaffolds based on collagen and supercritical fluids-assisted decellularized fibrous extracellular matrix. Polymers (Basel). 2021;**13**(24):4326

[18] Tappa K, Jammalamadaka U. Novel biomaterials used in medical 3D printing techniques. Journal of Functional Biomaterials. 2018;**9**(1):17

[19] Rhee S, Puetzer JL, Mason BN, Reinhart-King CA, Bonassar LJ. 3D bioprinting of spatially heterogeneous collagen constructs for cartilage tissue engineering. ACS Biomaterials Science & Engineering. 2016;**2**:1800-1805

[20] Laronda MM, Rutz AL, Xiao S, Whelan KA, Duncan FE, Roth EW, et al. A bioprosthetic ovary created using 3D printed microporous scaffolds restores ovarian function in sterilized mice. Nature Communications. 2017;**8**:15261

[21] Huang CC. Decellularized liver-regenerative 3D printing biomaterials for cell-based liver therapies via a designed procedure combining supercritical fluids with papain-containing reagents. Bio-medical Materials and Engineering. 2022;**33**(2):139-146

[22] Markstedt K, Mantas A, Tournier I, Martínez-Ávila H, Hägg D, Gatenholm P. 3D bioprinting human chondrocytes with nanocellulose–alginate bioink for cartilage tissue engineering applications. Biomacromolecules. 2015;**16**:1489-1496

[23] Li S, Tian X, Fan J, Tong H, Ao Q, Wang X. Chitosans for tissue repair and organ three-dimensional (3D) bioprinting. Micromachines (Basel). 2019;**10**(11):765

[24] Wang X, Wang Q, Xu C. Nanocellulose-based inks for 3D bioprinting: Key aspects in research development and challenging perspectives in applications: A mini review. Bioengineering (Basel). 2020;**7**(2):40

[25] Gong C, Kong Z, Wang X. The effect of agarose on 3D bioprinting. Polymers (Basel). 2021;**13**(22):4028

[26] Li JX, Zhao SX, Zhang YQ. Silk protein composite bioinks and their 3D scaffolds and in vitro characterization. International Journal of Molecular Sciences. 2022;**23**(2):910

[27] Nguyen D, Hägg DA, Forsman A, Ekholm J, Nimkingratan P, Brantsing C, et al. Cartilage tissue engineering by the 3D bioprinting of iPS cells in a nanocellulose/alginate bioink. Scientific Reports. 2017;**7**:658

[28] Petta D, D'Amora U, Ambrosio L, Grijpma DW, Eglin D, D'Este M. Hyaluronic acid as a bioink for extrusion-based 3D printing. Biofabrication. 2020;**12**(3):032001

[29] Lam T, Dehne T, Krüger JP, Hondke S, Endres M, Thomas A, et al. Photopolymerizable gelatin and hyaluronic acid for stereolithographic 3D bioprinting of tissue-engineered cartilage. Journal of Biomedical Materials Research. Part B, Applied Biomaterials. 2019;**107**(8):2649-2657

[30] Huang CC. New designed decellularized scaffolds for scaffold-based gene therapy from elastic cartilages via supercritical carbon dioxide fluid and alkaline/protease treatments. Current Gene Therapy. 2021

[31] Perez-Puyana V, Romero A, Guerrero A. Influence of collagen concentration and glutaraldehyde on

collagen-based scaffold properties. Journal of Biomedial Materials Research Part A. 2016;**104**:1462-1468

[32] Huang CC. Tuning gelatin–alginate bioink properties by introducing new decellularized elastic cartilage scaffolds for bioinspired composite membranes in orthopedics. Polymer Bulletin. 2022

[33] Baltazar T, Merola J, Catarino C, Xie CB, Kirkiles-Smith NC, Lee V, et al. Three dimensional bioprinting of a vascularized and perfusable skin graft using human keratinocytes, fibroblasts, pericytes, and endothelial cells. Tissue Engineering. Part A. 2020;**26**(5-6):227-238

[34] Huang CC. Design and characterization of a bioinspired polyvinyl alcohol matrix with structural foam-wall microarchitectures for potential tissue engineering applications. Polymers. 2022;**14**:1585

[35] Kasaj A, Reichert C, Götz H, Röhrig B, Smeets R, Willershausen B. In vitro evaluation of various bioabsorbable and nonresorbable barrier membranes for guided tissue regeneration. Head & Face Medicine. 2008;**4**:1-8

[36] Subhan F, Hussain Z, Tauseef I, Shehzad A, Wahid F. A review on recent advances and applications of fish collagen. Critical Reviews in Food Science and Nutrition. 2020;**61**:1027-1037

[37] Dattola E, Parrotta EI, Scalise S, Perozziello G, Limongi T, Candeloro P, et al. Development of 3D PVA scaffolds for cardiac tissue engineering and cell screening applications. RSC Advances. 2019;**9**:4246-4257

[38] Saavedra YG, Mateescu MA, Averill-Bates DA, Denizeau F. Polyvinylalcohol three-dimensional matrices for improved long-term dynamic culture of hepatocytes. Journal of Biomedical Materials Research. Part A. 2003;**66**:562-570

[39] Baker MI, Walsh SP, Schwartz Z, Boyan BD. A review of polyvinyl alcohol and its uses in cartilage and orthopedic applications. Journal of Biomedical Materials and Research B. 2012;**100**:1451-1457

[40] Hou Y, Xie W, Achazi K, Cuellar-Camacho JL, Melzig MF, Chen W, et al. Injectable degradable PVA microgels prepared by microfluidic technology for controlled osteogenic differentiation of mesenchymal stem cells. Acta Biomaterialia. 2018;**77**:28-37

[41] Chen CY, Kuo SM, Tarng YW, Lin KC. Immediate application of negative pressure wound therapy following lower extremity fap reconstruction in sixteen patients. Scientific Reports. 2021;**11**:21158

[42] Hamidabadi HG, Rezvani Z, Bojnordi MN, Shirinzadeh H, Seifalian AM, et al. Chitosan-intercalated montmorillonite/poly(vinyl alcohol) nanofibers as a platform to guide neuronlike differentiation of human dental pulp stem cells. ACS Applied Materials Interfaces. 2017;**9**:11392-11404

[43] Peppas NA, Stauffer SRJ. Reinforced uncrosslinked poly (vinyl alcohol) gels produced by cyclic freezing-thawing processes: A short review. Journal of Controlled Release. 1991;**16**:305-310

[44] Trimnell D, Shasha BS, Otey FHJ. The effect of α-amylases upon the release of trifluralin encapsulated in starch. Journal of Controlled Release. 1985;**1**:183-190

[45] Chang YI, Cheng WY, Jang L. A novel method of making PVF Porous foam without using the pore forming

agent. Journal of Applied Polymer Science. 2014;**132**:41270

[46] BeMiller JN, Whistler RL. Starch: Chemistry and Technology. 3rd ed. New York, NY, USA: Academic Press; 2009

[47] Wilson JD, Bechtel DB, Todd TC, Seib PA. Cereal Chemistry. 2006;**83**:259

[48] 48.Lan W, Xu M, Qin M, Cheng Y, Zhao Y, Huang D, et al. Physicochemical properties and biocompatibility of the bi-layer polyvinyl alcohol-based hydrogel for osteochondral tissue engineering. Materials and Design. 2021;**204**:109652

[49] Wu Z, Kong B. Engineering of corneal tissue through an aligned PVA/collagen composite nanofibrous electrospun scaffold. Nanomaterials. 2018;**8**:124-140

[50] 50.Barbon S, Contran M, Stocco E, Todros S, Macchi V, Caro RD, et al. Enhanced biomechanical properties of polyvinyl alcohol-based hybrid scaffolds for cartilage tissue engineering. PRO. 2021;**9**:730

[51] Iqbal B, Muhammad N, Rahim A, Iqbal F, Sharif F, Safi SZ, et al. Development of collagen/PVA composites patches for osteochondral defects using a green processing of ionic liquid. International Journal of Polymeric Materials. 2019;**68**:590-596

[52] Choi SM, Singh D, Kumar A, Oh TH, Cho YW, Han SS. Porous three-dimensional PVA/gelatin sponge for skin tissue engineering. International Journal of Polymeric Materials and Polymeric Biomaterials. 2013;**62**:384-389

[53] Kamoun EA, Kenawy ER, Chen SX. A review on polymeric hydrogel membranes for wound dressing applications: PVA-based hydrogel dressings. Journal of Advanced Research. 2017;**8**:217-233

[54] Sionkowska A. Current research on the blends of natural and synthetic polymers as new biomaterials: Review. Progress in Polymer Science. 2011;**36**:1254-1276

[55] Min Q, Tian D, Zhang Y, Wang C, Wan Y, Wu J. Strong and elastic chitosan/silk fibroin hydrogels incorporated with growth-factor-loaded microspheres for cartilage tissue engineering. Biomimetics. 2022;**7**:41

[56] Reddy R, Reddy N. Biomimetic approaches for tissue engineering. Journal of Biomaterials Science. Polymer Edition. 2018;**29**:1667-1685

[57] Ngadimin KD, Stokes A, Gentile P, Ferreira AM. Biomimetic hydrogels designed for cartilage tissue engineering. Biomaterials Science. 2021;**9**:4246-4259

[58] Niu W, Xiao Q, Wang X, Zhu J, Li J, Liang X, et al. A biomimetic drug delivery system by integrating grapefruit extracellular vesicles and doxorubicin-loaded heparin-based nanoparticles for glioma therapy. Nano Letters. 2021;**21**:1484-1492

[59] Ziai Y, Petronella F, Rinoldi C. Chameleon-inspired multifunctional plasmonic nanoplatforms for biosensing applications. NPG Asia Materials. 2022;**14**:18

[60] Lingham-Soliar T. Feather structure, biomechanics and biomimetics: The incredible lightness of being. Journal für Ornithologie. 2014;**155**:323-336

[61] Bonser RHC. The mechanical performance of medullary foam from feathers. Journal of Materials Science Letters. 2001;**20**:941-942

[62] Aldemir DB, Claeyssens F. Basic principles of emulsion templating and its use as an emerging manufacturing method of tissue engineering scaffolds. Frontiers in Bioengineering and Biotechnology. 2020;**8**:875

[63] Bak TY, Kook MS, Jung SC, Kim BH. Biological effect of gas plasma treatment on CO_2 gas foaming/salt leaching fabricated porous polycaprolactone scaffolds in bone tissue engineering. Journal of Nanomaterials. 2014;**3**:1-6

[64] Dikici S, Claeyssens F, MacNeil S. Bioengineering vascular networks to study angiogenesis and vascularization of physiologically relevant tissue models in Vitro. ACS Biomaterials Science & Engineering. 2020;**6**:3513-3528

[65] Dikici A, Dikici BS, Karaman O, Oflaz H. The effect of zinc oxide doping on mechanical and biological properties of 3D printed calcium sulfate based scaffolds. Biocybernetics Biomedical Engineering. 2017;**37**:733-741

[66] Richez A, Deleuze H, Vedrenne P, Collier R. Preparation of ultra-low-density microcellular materials. Journal of Applied Polymer Science. 2005;**96**:2053-2063

[67] Loh QL, Choong C. Three-dimensional scaffolds for tissue engineering applications: Role of porosity and pore size. Tissue Engineering. Part B, Reviews. 2013;**19**:485-502

[68] Despa F, Orgill DP, Neuwalder J, Lee RC. The relative thermal stability of tissue macromolecules and cellular structure in burn injury. Burns. 2005;**31**:568-577

[69] Rynkowska E, Fatyeyeva K, Marais S, Kujawa J, Kujawski W. Chemically and thermally crosslinked PVA-based membranes: Effect on swelling and transport behavior. Polymers. 1799;**2019**:11

[70] Obanni M, Bemiller JN. Properties of some starch blends. Cereal Chemistry. 1997;**74**:431-436

[71] Jacobs H. Influence of annealing on the pasting properties of starches from varying botanical sources. Cereal Chemistry. 1995;**72**:480-487

[72] Ratnayake WS, Otani C, Jackson DS. DSC enthalpic transitions during starch gelatinization in excess water, dilute sodium chloride, and dilute sucrose solutions. Journal of the Science of Food and Agriculture. 2009;**89**:2156-2164

[73] Beninca C, Colman TAD, Lacerda LG, Filho MASC, Demiate IM, Bannach G, et al. Thermal, rheological, and structural behaviors of natural and modified cassava starch granules, with sodium hypochlorite solutions. Journal of Analytical Calorimetry. 2013;**111**:2217-2222

[74] Hamdan S, Hashim DMA, Ahmad M, Embong S. Compatibility studies of polypropylene (PP)-sago starch (SS) blends using DMTA. Journal of Polymer Research. 2000;**7**:237-244

[75] Tao TX, Wu ZC, Wang XQ, Li MS, Zhang JH. Synthesis and spectra of compleses involving polyvinyl alcohol fiber ligands. Acta Polymerica Sinica. 2006;**3**:387-390

[76] Kizil R, Irudayaraj J, Seetharaman K. Characterization of irradiated starches by using FT-Raman and FTIR spectroscopy. Journal of Agricultural and Food Chemistry. 2002;**50**:3912-3918

[77] Dankar I, Haddarah A, Omar FEL, Sepulcre F. Influence of storage under unfavourable conditions on the caking properties and fungal contamination

of potato starch and wheat flour. Food Chemistry. 2018;**260**:7-12

[78] Abdullah AHD, Chalimah S, Primadona I, Hanantyo MHG. Physical and chemical properties of corn, cassava, and potato starchs. Earth and Environmental Science. 2018;**160**:012003

[79] Li J, Zeng H, Zeng Z, Zeng Y, Xie T. Promising graphene-based nanomaterials and their biomedical applications and potential risks: A comprehensive review. ACS Biomaterials Science & Engineering. 2021;**7**:5363-5396

[80] Sahana; T.G.; Rekha, P.D. Biopolymers: Applications in wound healing and skin tissue engineering. Molecular Biology Reports , 2018, 45, 2857-2867.

[81] Lee JS, Cho SW. Liver tissue engineering: Recent advances in the development of a bio-artificial liver. Biotechnol Bioproc E. 2012;**17**:427-438

[82] Zhang Q, Wang Q, Lv S, Lu J, Jiang S, Regenstein JM, et al. Comparison of collagen and gelatin extracted from the skins of Nile tilapia (Oreochromis niloticus) and channel catfish (Ictalurus punctatus). Food Bioscience. 2016;**13**:41-48

[83] Karimi A, Navidbakhsh M, Beigzadeh B. A visco-hyperelastic constitutive approach for modeling polyvinyl alcohol sponge. Tissue & Cell. 2014;**46**:97-102

[84] Stampella A, Papi A, Rizzitelli G. Synthesis and characterization of a novel poly(vinyl alcohol) 3D platform for the evaluation of hepatocytes response to drug administration. Journal of Materials Chemistry B. 2013;**2**:1-37

[85] Jain E, Damania A, Shakya AK. Fabrication of macroporous cryogels as potential hepatocyte carriers for bioartificial liver support. Colloids and Surfaces. B, Biointerfaces. 2015;**136**:761-771

[86] Jiang X, Christopherson GT, Mao HQ. The effect of nanofibre surface amine density and conjugate structure on the adhesion and proliferation of human haematopoietic progenitor cells. Interface Focus. 2011;**1**:725-733

[87] Xu S, Gu M, Wu K, Li G. Unraveling the interaction mechanism between collagen and alcohols with different chain lengths and hydroxyl positions. Colloids and Surfaces. B, Biointerfaces. 2021;**199**:111559

[88] Lai G, Du Z, Li G. The rheological behavior of collagen dispersion/poly(vinyl alcohol) blends. Korea-Austin Rheological Journal. 2007;**19**:81-88

[89] Zhou T, Zheng K, Sui B, Boccaccini AR, Sun J. In vitro evaluation of poly (vinyl alcohol)/collagen blended hydrogels for regulating human periodontal ligament fibroblasts and gingival fibroblasts. International Journal of Biological Macromolecules. 2020;**163**:1938-1946

[90] Lan W, Xu M, Zhang X, Zhao L, Huang D, Wei X, et al. Biomimetic polyvinyl alcohol/type II collagen hydrogels for cartilage tissue engineering. Journal of Biomaterials Science. Polymers. 2020;**31**:1-22

[91] Asran AS, Henning S, Michler GH. Polyvinyl alcohol–collagen–hydroxyapatite biocomposite nanofibrous scaffold: Mimicking the key features of natural bone at the nanoscale level. Polymer. 2010;**51**:868-876

[92] Majhy B, Priyadarshini P, Sen AK. Effect of surface energy and roughness on cell adhesion and growth–facile

surface modification for enhanced cell culture. RSC Advances. 2021;**11**:15467-15476

[93] Moscato S, Ronca F, Campani D. Poly(vinyl alcohol)/gelatin hydrogels cultured with HepG2 Cells as a 3D model of hepatocellular carcinoma: A morphological study. Journal of Functional Biomaterials. 2015;**6**:16-32

[94] Lei X, Zhang G, Yang MJ, Du Y, Huang CC. Morphology of novel chitosan oligosaccharides modified cross-linked polyvinyl alcohol complex foam (COS/cPVACF) dressings with fully open-cell and open-channel microstructures via active molecules cleaning process for wound managements. Biomedical Journal of Scientific & Technical Research. 2019;**17**(3):12819-12823

[95] Huang CC, Wu XW, Hsieh YL, Lin MH, Li J, Du Y, et al. Preparation and preclinical evaluations of deigned polymeric chitosanoligosaccharide (COS)/chitosan composite microcapsules with uniform sizes as a novel control released carrier via premixed membrane emulsification. Basic & Clinical Pharmacology & Toxicology. 2020;**126**(1):66

[96] Huang CC, Lin MH, Hsieh YL, Wu XW, Li J, Du Y, et al. Production and preclinical evaluation of designed chitosanoligosaccharide surface-modified microcapsules with uniform size in aqueous dispersions as a novel control released carrier via premixed membrane emulsification. Basic & Clinical Pharmacology & Toxicology. 2020;**126**(1):67

[97] Wang X, Chung YS, Lyoo WS, Min BG. Preparation and properties of chitosan/poly(vinyl alcohol) blend foams for copper adsorption. Polymer International. 2006;**55**(11):1230-1235

[98] Huang CC. Establishment of BM-TRIZ biomedical inventive principles and design-thinking methods for innovative design of medical devices based on a new polymeric biomaterial containing polyvinyl alcohol foam via an air-foaming procedure. Annals of Advanced Biomedical Sciences (AABSc). 2021;**4**(1):1-12